Scaling and optimization of the radiation temperature in dynamic hohlraums

S. A. Slutz, M. R. Douglas, J. S. Lash, R. A. Vesey, G. A. Chandler, T. J. Nash, and M. S. Derzon
Sandia National Laboratories, Albuquerque, New Mexico 87185-1186

(Received 22 August 2000; accepted 8 February 2001)

A quasianalytic model of the dynamic hohlraum is presented. Results of the model are compared to both experiments and full numerical simulations with good agreement. The computational simplicity of the model allows one to find the behavior of the hohlraum radiation temperature as a function of the various parameters of the system and thus find optimum parameters as a function of the driving current. The model is used to investigate the benefits of ablative standoff and quasispherical Z pinches. © *2001 American Institute of Physics.* [DOI: 10.1063/1.1360213]

I. INTRODUCTION

Pulsed power is a robust and inexpensive technology for obtaining high electrical energy densities, which can be efficiently converted into thermal radiation by Z pinches. The use of wire arrays, with a large number of wires, has resulted in remarkable improvements in radiated power from Z pinches. Recently,[1] 2 MJ of thermal x rays have been generated by a Z pinch with an efficiency greater than 15% and an x-ray power exceeding 200 TW. This thermal x-ray power has been used to drive a hohlraum[2] to a temperature greater than 145 eV. A promising inertial fusion scenario[3] is to use two Z pinches to drive an external hohlraum containing a fusion capsule as shown in Fig. 1. Calculations[3] indicate that high yields (400–1200 MJ) can be obtained with 16 MJ of x-ray energy provided by the two pinches. A large fraction of the x-ray energy is absorbed by the hohlraum walls of the primary and secondary hohlraums, which have an area of approximately 30 cm^2.

The dynamic hohlraum[4] is an alternative approach to generating thermal radiation to drive a capsule, which should require less total energy. In this approach, a Z-pinch plasma is imploded onto a ''convertor,'' which surrounds the capsule as depicted schematically in Fig. 2. In Fig. 2, the Z-pinch plasma is initially formed at r_{Z0} and is imploded onto the convertor, which initially occupies the region $r_{ci} < r < r_{co}$. The Z-pinch plasma can be generated from a wire array or a solid liner. The implosion velocity of the Z pinch must be sufficiently high (>20 cm/μs) to efficiently generate radiation. To obtain these velocities the Z pinch must be low mass (few milligrams) for the present machine. This explains why wires have been the most successful since low mass liners cannot be constructed without wrinkles, which seed the Rayleigh–Taylor instability. The mass of the Z pinch can be increased with larger driving current, so liners may become practical at the higher currents needed to drive fusion capsules.

When the Z-pinch plasma first strikes the convertor it is in the region $r_{co} < r < r_{Z0}$, see Fig. 2. The radius of interface between the Z-pinch plasma and the convertor, r_{Zi}, is r_{co} at first contact. Two shock waves are formed at r_{co}, one propagates into the Z-pinch plasma and the other propagates inward into the convertor. These shock waves heat both regions, which then emit thermal radiation. A material of low opacity (typically a plastic foam) is chosen for the convertor so that radiation can easily flow inward to heat an inertial confinement fusion (ICF) capsule. Note the opacity must not be too low or the material would not radiate effectively. Numerical simulations show that there are materials such as plastic foams that satisfy both conditions. The Z-pinch plasma is composed of a material with high opacity (tungsten is commonly used) to minimize the outward flow of radiation and thus achieve maximal hohlraum radiation temperatures. The Z-pinch plasma forms the walls of a hohlraum with much smaller dimensions (several millimeters) than the walls of the double-ended Z-pinch driven hohlraum ($\sim$1 cm). Thus we expect the dynamic hohlraum to have less radiation loss and to generate higher radiation temperatures than would be obtained using the double-ended Z-pinch driven hohlraum with the same total energy. Indeed, numerical simulations[5] indicate that a dynamic hohlraum could drive a high yield capsule (500 MJ) with approximately 6 MJ of kinetic energy delivered to the Z pinch. This is roughly 40% of the kinetic energy that would be required for the double-ended Z-pinch driven hohlraum. Furthermore, the performance of the dynamic hohlraum depends on the tradeoff between a number of factors, with the likelihood that this design has not been fully optimized. Therefore it is valuable to have a model to determine the performance of the dynamic hohlraum as a function of the many parameters that can be varied. A simple analytic estimate[6] of the peak hohlraum radiation temperature based on shock heating has been made. We present a more complete model that includes the effects of radiation loss, the specific heat of the components, and the radiation absorbed by the capsule. We use our model to find optimum parameters as a function of the driving current.

The model also includes the effects of ablative standoff, where incoming shock waves can be isolated from the capsule by the outgoing ram pressure of the ablated material. This effect has been seen in numerical simulations[5] of high yield dynamic hohlraum driven capsules. We find that abla-

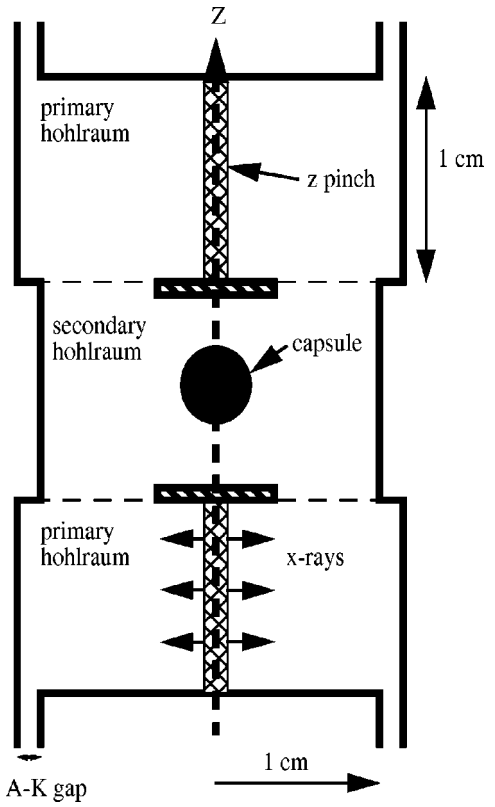

FIG. 1. A schematic of a double-ended Z-pinch-driven hohlraum.

tive standoff is more effective at larger drive currents.

A quasispherical Z-pinch implosion of an initially cylindrical Z pinch will occur if the Z-pinch material has an appropriate axial mass profile, i.e., heavier at the midplane and lighter at the ends. We have performed both simplified and detailed numerical simulations of an initially cylindrical Z pinch with a 2 cm initial radius and 1 cm initial axial length, that had a mass/length, Λ, given by

$$\Lambda = \Lambda_0(1 + a_2 Z^2 + a_4 Z^4), \tag{1}$$

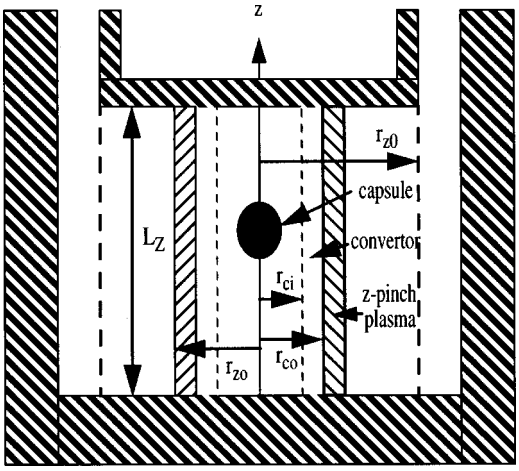

FIG. 2. A schematic of a dynamic hohlraum. The Z-pinch plasma is shown at the time of first impact with the convertor. The initial inner and outer radius of the convertor are labeled r_{ci} and r_{co}.

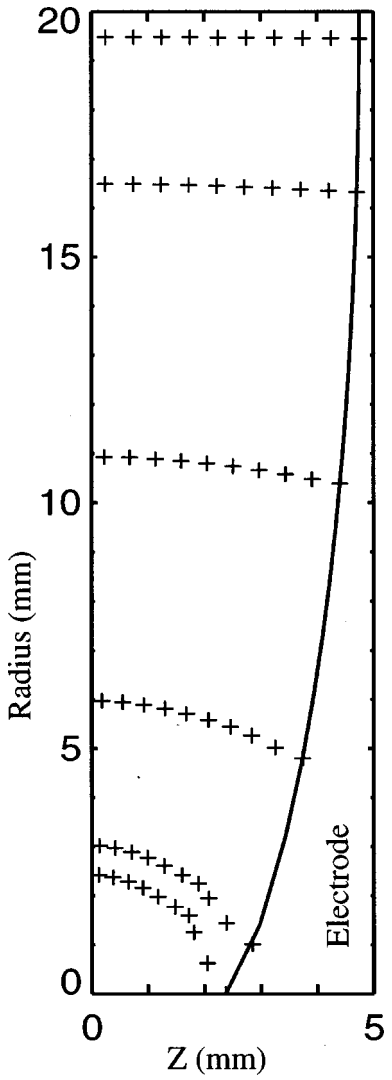

FIG. 3. Numerical solution for a quasi-spherical Z pinch at several times. The simplified model is described in Sec. V C.

where $a_2 = -0.06$, $a_4 = 0.024$, and $\Lambda_0 = 3.75$ mg/cm. The results from the simplified model at various times during the implosion are shown in Fig. 3. The crosses are points along the Z pinch. The shape of the electrode is found from the trajectory of the point of the Z pinch furthest from the midplane. As can be seen the final shape is nearly spherical. Note that the radius when the pinch becomes quasispherical can be adjusted by changing the mass profile, the pinch length, and the initial pinch radius. This adjustment will be necessary for different convertor radii. Similar results have been obtained by others.[7] This quasispherical Z-pinch implosion should provide better coupling to the spherical inertial fusion capsule. Indeed, our model predicts significantly higher hohlraum temperatures for quasispherical Z-pinch implosions than for purely cylindrical Z-pinch implosions. However, as we shall show with numerical simulations, the mass profile needed to produce a quasispherical implosion also seeds the Rayleigh–Taylor instability. Experiments will be needed to determine the viability of quasispherical Z-pinch implosions.

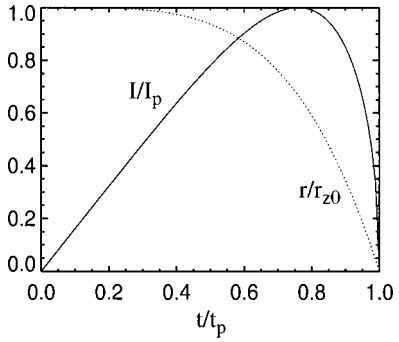

FIG. 4. Analytic solution for the normalized drive current and Z-pinch radius for a cylindrical pinch as a function of time normalized to the final pinch time, t_p.

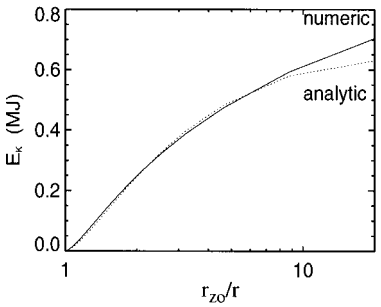

FIG. 5. A comparison between the analytic solution (dotted line) and a numerical solution (solid line) for the kinetic energy of a cylindrical Z pinch as a function of the Z-pinch convergence ratio.

This paper is organized as follows. The model of the dynamic hohlraum is presented in the Sec. II. Results are compared to experiments in Sec. III. In Sec. IV, model results are compared to full radiation hydrodynamic simulations to further benchmark the model. In Sec. V, the model is then used to optimize and predict the scaling of dynamic hohlraums. Conclusions are given in Sec. VI. The analytic Z-pinch model is described in Appendix A. The radiation transport through the Z-pinch plasma is described in Appendix B. A glossary of symbol definitions is provided in Appendix C.

II. DYNAMIC HOHLRAUM MODEL

A. Analytic Z-pinch solutions

We are interested in modeling both purely cylindrical and quasispherical Z-pinch implosions. Analytic solutions for purely cylindrical and quasispherical Z pinches are developed in Appendix A. The normalized radius and current for a cylindrical pinch are plotted as a function of time in Fig. 4. The initial mass of the Z pinch is found to be

$$M_Z=\frac{(3-2\alpha)^{2-\alpha}}{12(2-2\alpha)^{1-\alpha}}\left(\frac{\mu_0}{4\pi}\right)\left(\frac{I_p t_r}{r_{Z0}}\right)^2 L_Z, \tag{2}$$

where I_p is the peak driving current, t_r is the rise time, L_Z is the initial length of the pinch, r_{Z0} is the initial radius of the pinch, and α is a parameter which determines the degree of axial convergence. Cylindrical pinches correspond to $\alpha=0$, while the quasispherical Z pinch shown in Fig. 3 corresponds to $\alpha=1/3$.

The kinetic energy of the Z pinch is found to be

$$E_K=\frac{2(3-2\alpha)^{3/2-\alpha}}{3(2-2\alpha)^{1-\alpha}}L_Z\left(\frac{\mu_0}{4\pi}\right)I_p^2\left(1-\frac{r}{r_{Z0}}\right)^{3/2}, \tag{3}$$

where r is the radius of the Z pinch. A comparison between Eq. (3) ($\alpha=0$) with a cylindrical numerical solution, which includes inductive feed back on the current, is shown in Fig. 5. The agreement is excellent for convergence ratios expected in dynamic hohlraums, i.e., less than 5. The analytic solution facilitates optimization, which involves finding many solutions.

B. Hohlraum temperature profile

The collision between the Z-pinch plasma and the convertor generates shocks which propagate through both the Z-pinch plasma and the convertor. These shocks heat both the Z-pinch plasma and the convertor material to high temperatures, which then emit thermal x rays. Some of these x rays are absorbed by the fusion capsule, some are absorbed by the electrodes, and some of them travel radially outward through the Z-pinch material to be lost. The radiation lost through the Z-pinch plasma is minimized by using a high opacity material such as tungsten. The radiation temperature will have a large spatial gradient within the Z-pinch plasma due to the high opacity. The transport of the radiation is calculated in Appendix B. In contrast, the convertor material is chosen to have relatively low opacity, e.g., plastic foam is commonly used. This allows the radiation to travel freely toward the fusion capsule with only a small radiation temperature gradient within the convertor material. Note that the opacity of the convertor material should not be too low or it would not effectively radiate. Numerical simulations show that low Z materials such as plastic foam can satisfy both requirements. In these simulations the material temperature just behind the incoming shock wave can be substantially larger than the radiation temperature. Increasing the opacity of the convertor material with high-Z dopants will reduce this difference, but too high an opacity will impede the radiation flow inward toward the capsule. Simulations indicate that undoped plastic foams yield nearly optimal performance.

We define the hohlraum temperature to be the average radiation temperature within the region bounded by the interface between the Z-pinch plasma and the convertor. We shall consider two basic convertor geometries, annular and solid convertors. Note the hohlraum includes a region of vacuum for annular convertors.

For annular convertors the shocks will pass completely through the convertor and the Z-pinch plasma before the convertor implodes on axis. The convertor and the Z-pinch plasma will then be at high pressure and thus difficult to compress further. The magnetic pressure will still accelerate the Z-pinch plasma and the convertor inward, but this kinetic energy will not be turned into heat until stagnation on the axis. Therefore little heating will occur after the initial

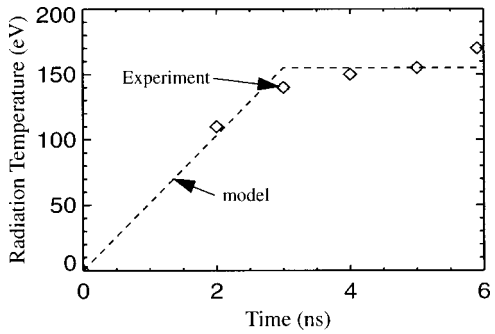

FIG. 6. Experimentally measured hohlraum temperature for shot 417, which used an annular copper convertor with an initial radius of 4 mm and a thickness of 2 μm. This is compared to a curve (dashed line) that rises linearly to a maximum value and then remains constant.

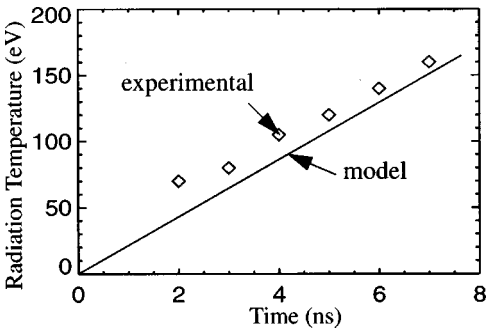

FIG. 7. Experimentally measured hohlraum radiation temperature as a function of time for shot 291 (diamonds) compared to model calculations (solid line). The foam convertor had an initial radius of 4 mm with a density of 6 mg/cc.

shocks have passed through the convertor and the Z-pinch plasma, but before final stagnation on axis. Thus we expect the hohlraum temperature to reach a peak when the shock has just passed through the convertor and then the hohlraum temperature will decrease slowly as the convertor continues to collapse inward. A sharp rise in the radiation temperature occurs when the convertor and the Z-pinch plasma stagnate on axis, but the fusion capsule must implode before this or it will be crushed nonspherically and not reach sufficient compression to ignite the fusion reaction. Thus we shall not include the stagnation phase of the radiation temperature profile in our model of the hohlraum temperature profile.

The initial radius of the convertor must be chosen so that stagnation occurs after the fusion capsule implodes. Experimental measurements of the radiation temperature within an annular convertor are consistent with this description, see Fig. 6. In our model, we shall approximate this behavior by assuming the hohlraum temperature rises linearly with time up to its peak value, T_{HP}, in a rise time, τ_r, then stays constant until the capsule implodes, which we refer to as the capsule bang time, $\tau_b=\tau_r+\tau_{\mathrm{cap}}$. The rise time is determined by the time it takes for the stagnation shock to pass through the convertor and the Z-pinch plasma. This time is short compared to the capsule implosion time so the details of the radiation temperature rise should not be important.

The high yield design[5] uses a foam convertor that extends to the axis, i.e., the capsule is imbedded in the foam. As our calculations will reveal, the mass of the convertor will be comparable to the mass of the Z-pinch plasma for optimal performance. Since the outer radius of the convertor must be large enough to provide radiation early enough to drive the capsule before the Z pinch implodes on the capsule, a low density material such as foam must be used for a solid convertor. Solid convertors result in rising hohlraum temperature during the entire capsule implosion. Such convertors also couple more of the stagnation energy into the convertor and the relatively slow rise of the hohlraum temperature yields a reasonably isentropic implosion of the fusion capsule. Figure 7 shows the experimentally measured radiation temperature for a solid foam convertor. As can be seen the radiation temperature rises approximately linearly with time. Thus we will assume that for solid convertors the radiation temperature is given by the expression, $T_H(t)=tT_{\mathrm{HP}}/\tau_b$, where $\tau_b=\tau_{\mathrm{cap}}$ for solid convertors. Again the initial outer radius of the foam must be chosen so that the Z-pinch material does not stagnate on the capsule before it implodes, since this would destroy the capsule symmetry.

C. Capsule implosion time

We shall now estimate the capsule implosion time as a function of the initial radius and final implosion velocity. Assuming that most of the capsule mass is contained in a hollow shell, Newton's equation for the radius of a capsule during implosion can be written

$$m_{\mathrm{cap}}(r_c)\frac{d^2r_c}{dt^2}+4\pi r_c^2P_{\mathrm{abl}}=0, \tag{4}$$

where r_c is the radius of the capsule as a function of time, $m_{\mathrm{cap}}(r_c)$ is the unablated capsule mass. We approximately account for the decrease in the capsule mass due to ablation by assuming, $m_{\mathrm{cap}}(r)=M_{\mathrm{cap}}(r/r_{\mathrm{cap}})^2$, where M_{cap} is the initial capsule mass and r_{cap} is the initial capsule radius. This form is convenient since it admits exact analytic solutions. We have found the implosion time to be weakly dependent on this assumption. The ablation pressure at the surface of an inertial fusion capsule is approximately[8]

$$P_{\mathrm{abl}}=3.3\times10^4T_H^{3.5}, \tag{5}$$

where T_H is the radiation temperature in units of electron volts and the ablation pressure is in pascals.

For annular convertors, we will ignore the rising portion of the temperature profile, since it is typically short compared to the capsule implosion time. Assuming a constant hohlraum temperature during the capsule implosion, Eq. (4) can be solved exactly. The implosion time is then found to be

$$\tau_{\mathrm{cap}}=\frac{2r_{\mathrm{cap}}}{v_f}. \tag{6}$$

For solid low density convertors, we assume a linear rise in the hohlraum temperature until the capsule implosion time. Equation (4) can be solved assuming a linear rise in the hohlraum temperature, with the result

$$\tau_{\mathrm{cap}}=\frac{5.5r_{\mathrm{cap}}}{v_f}. \tag{7}$$

The final implosion velocity, v_f, of an inertial fusion capsule must be approximately 35 cm/μs to obtain ignition.[8]

D. Geometric considerations and radiation symmetry

Numerical simulations indicate that inertial fusion capsules require a radiation flux asymmetry of 1% or less.[8] Thus there must be sufficient space between the Z-pinch plasma and the capsule so that the radiation can transport freely around the capsule to provide a symmetric radiation drive. This condition is satisfied if the Z-pinch/convertor interface radius is larger than some minimum radius during the capsule implosion. We define a symmetry parameter

$$F_s=\frac{r_{\mathrm{Zib}}}{r_{\mathrm{cap}}}, \tag{8}$$

where r_{Zib} is the inner radius of the Z-pinch plasma at capsule implosion time (bang time). Large values of F_s will allow a high degree of radiation smoothing, but will also result in relatively low hohlraum temperatures. Thus it is important to have at least an estimate of the minimum value of F_s that is consistent with the required radiation symmetry. Note that F_s can be less than unity because the capsule is imploding as the inner radius of the Z-plasma decreases and r_{cap} is defined to be the initial capsule radius.

Numerical simulations using the code LASNEX[9] show that the Rayleigh–Taylor (RT) instability modulates the Z-pinch plasma thickness with a wavelength of approximately 1 mm, see Fig. 8. These simulations indicate that the RT instability induced radiation source has a variation, $\delta T^4/T^4\sim 30\%$ for the dominant wavelength of approximately 1 mm. Note however, that the amplitude is not the same for each bubble and spike. This indicates the presence of longer wavelengths.

The radiation flux incident on the capsule surface can be much more uniform than the radiation source at the Z-pinch plasma, which acts as the hohlraum wall. This is because radiation incident on each point of the capsule is a solid angle weighted integral over the visible hohlraum wall. We have performed these integrals in a ''view factor'' code. The hohlraum wall and the radiation source were assumed to be a cylinder with a radius of R_{hohl} and length L_{hohl} with a constant ratio $L_{\mathrm{hohl}}/R_{\mathrm{hohl}}=4$. The radiation flux emitted from the hohlraum wall was given a sinusoidal axial variation with a fixed wavelength to simulate the effect of the RT instability. The albedo of the walls was set to zero (due to the lack of a self-consistent wall loss model), which results in an underestimate of the effect of radiation smoothing.

Calculations were performed for several values of the ratio R_{hohl}/R_c, and the source wavelength, λ/R_c, for fixed relative variation of the source amplitude, $\delta F/F_0$, where F_0 is the source amplitude without any variations due to RT and R_c is the capsule radius at the time of interest during its implosion. Calculations with $\delta F/F_0=0$ result in a 34% variation of the radiation flux at the capsule from equator to pole. This unperturbed equator to pole variation results from the end walls (the electrodes), which are not radiation sources. This variation is reduced as the electrode albedo is increased to reasonable values for gold (albedo=0.8 gives a 6% variation). The remaining variation, which should be the same on each shot, can in principle be compensated for by design. Possible solutions, such as using a quasispherical implosion to avoid the cold end walls, need to be explored.

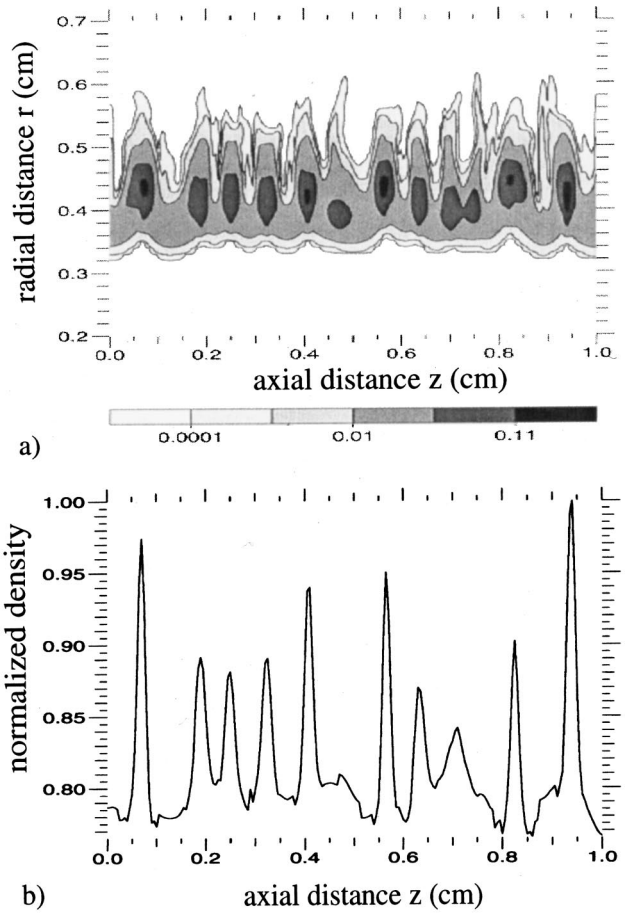

FIG. 8. Results of a 2-D numerical simulation of a Z pinch stagnating onto a plastic convertor, (a) radiation temperature contours, (b) line out of the density as a function of axial distance Z at a fixed radius $r=4$ mm.

In contrast, the variation caused by the RT instability will be different on each shot. To assess the effect of the RT instability, we subtracted this unperturbed variation from calculations with the sinusoidal perturbations and expanded the results into Legendre modes. Since fusion capsules require a time averaged radiation flux asymmetry of 1% or better (summed over all modes), we inverted our results to find the required source amplitude to obtain 1% variation on the capsule, δF_1, as a function of the ratio R_{hohl}/R_c. The results are plotted in Fig. 9 for three different wavelengths, $\lambda=1$, 2, and 4 mm. Note $R_c=1$ mm for these calculations. The results are applicable to other capsule sizes by scaling the wavelength with the capsule size. As can be seen from Fig. 9, δF_1 is a strong function of both R_{hohl}/R_c and the wavelength. The results indicate that for $\lambda=1$ mm, source variations of 30% seen in the LASNEX simulations should be smoothed to approximately 1% at the capsule for the ratio $R_{\mathrm{hohl}}/R_c=2.0$. Adequate radiation symmetry will be achieved if the ratio of

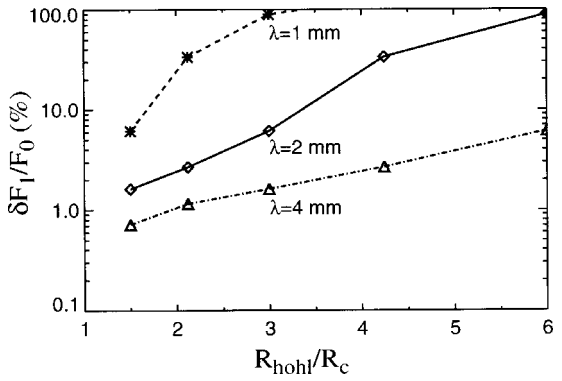

FIG. 9. The source flux variation that yields a 1% radiation flux asymmetry at the capsule, as calculated by view factor simulations, is plotted as a function of the hohlraum radius, R_{hohl}, over the capsule radius, R_c. The curves are labeled by the wavelength of the RT instability assuming $R_c = 1$ mm.

the inner radius of the Z-pinch plasma over the capsule radius is never smaller than approximately 2. We have solved Eq. (4) to determine the capsule radius as a function of time. Comparing this to the radius of the Z pinch as a function of time we find that a ratio $F_s > 0.5$ is usually large enough to ensure this condition is satisfied. Note that the LASNEX simulations show that the RT introduces some structure at wavelengths longer than 1 mm. If such longer wavelength modes have sufficient amplitude in the experiments, larger values of F_s may be needed to obtain adequate radiation symmetry.

We can calculate the initial outer radius of the convertor to obtain a desired value of the symmetry parameter from the simple formula

$$r_{\mathrm{co}} \approx F_s r_{\mathrm{cap}} + \overline{v}_{\mathrm{Zp}} \tau_{\mathrm{cap}}, \tag{9}$$

where $\overline{v}_{\mathrm{Zp}}$ is the average velocity of the of the inner surface of the Z-pinch plasma from the time of first contact with the convertor until the capsule has fully imploded (bang time).

We have an analytic solution [Eq. (A8)] for the velocity of the Z pinch in the absence of the convertor. Let v_1 be the velocity of the Z pinch at the initial outer radius of the convertor, r_{co}, and let v_2 be the velocity at the desired final position $r_{\mathrm{Zib}} = F_s r_{\mathrm{cap}}$, when the capsule is fully imploded. We shall use these two velocities to obtain approximate expressions for the average velocity of the inner surface of the Z-pinch plasma when a convertor is present. The result will be different for annular and solid convertors.

First consider annular convertors. We assume that the collision between the Z-pinch plasma and the convertor is essentially inelastic. The velocity of the Z-pinch plasma/convertor after the collision is then approximately

$$v_{\mathrm{coll}} = \frac{M_{\mathrm{Z}}}{(M_{\mathrm{Z}} + M_c)} v_1. \tag{10}$$

As the convertor implodes the magnetic pressure will increase the implosion velocity. This increased kinetic energy will be approximately the same as the energy gained by an imploding Z pinch without a convertor given by

$$\Delta E = \frac{M_{\mathrm{Z}}}{2}(v_2^2 - v_1^2). \tag{11}$$

This would be rigorously true if the driving current were unaffected by the Z-pinch collision with the convertor. The velocity of the Z-pinch/convertor interface at r_{Zib} (bang time) will then be approximately

$$v_{\mathrm{bang}} = \left(v_{\mathrm{coll}}^2 + \frac{2\Delta E}{M_c + M_{\mathrm{Z}}} \right)^{1/2}. \tag{12}$$

The average velocity is then simply

$$\overline{v}_{\mathrm{Zp}} = \frac{v_{\mathrm{coll}} + v_{\mathrm{bang}}}{2}. \tag{13}$$

The situation is different for a solid convertor, where the collision occurs during the entire implosion. Assuming that the shock has propagated through all of the convertor by the time the Z-pinch/convertor radius reaches r_{Zib} the velocity at bang time will be approximately

$$v_{\mathrm{bang}} = \frac{v_2 M_{\mathrm{Z}}}{M_{\mathrm{Z}} + M_c}. \tag{14}$$

The average velocity is then

$$\overline{v}_{\mathrm{Zp}} = \tfrac{1}{2}(v_1 + v_{\mathrm{bang}}), \tag{15}$$

which can be substituted into (9) to find r_{co}.

E. Ablative standoff

For solid convertors, a shock wave can arrive at the capsule before bang time. This is a potential problem, because the shock wave could disrupt the spherical symmetry of the fusion capsule. However, under appropriate conditions, the ablation pressure is larger than the shock pressure and the shock will remain isolated from the capsule. We call this ablative standoff. The pressure of the shock wave is given by[10]

$$P_{\mathrm{sh}} = \frac{2\rho_c v_s^2}{\gamma + 1}, \tag{16}$$

where ρ_c is the initial convertor density. The Z-pinch plasma acts as a piston driving a shock wave into the convertor. The shock wave will move ahead of the interface. Assuming an ideal gas with $\gamma = 5/3$, the shock will move at 4/3 times the velocity of the interface. In addition the shock will be accelerated by cylindrical or spherical convergence. Analytic solutions[11] show that the shock velocity is proportional to $r^{-\mu}$ where $\mu = 0.226$ for cylindrical and $\mu = 0.45$ for spherical convergence. Thus the velocity of the shock is approximately

$$v_s = \frac{4\overline{v}_{\mathrm{Zp}}}{3}\left(\frac{r_{\mathrm{co}}}{r}\right)^{\mu}. \tag{17}$$

The ablation pressure generates an outward flow of material which has a ram pressure given by

$$P_{\mathrm{ram}} = \left(\frac{r_{\mathrm{cap}}}{r}\right)^2 P_{\mathrm{abl}}, \tag{18}$$

where r_{cap} is the initial capsule radius and P_{abl} is found from Eq. (5). Note that the capsule will not have imploded much at the time that the first shock arrives at the capsule. Setting

$P_{ram}=P_{sh}$, we define r_{ab}/r_{cap}, the ablative standoff radius (point where the ram pressure equals the shock pressure) normalized to the capsule radius. The result is

$$\frac{r_{ab}}{r_{cap}}=\frac{210}{v_s\sqrt{\rho_c}}T_{HS}^{1.75}, \tag{19}$$

where T_{HS}, the hohlraum temperature at the time when the shock reaches the capsule, is given by

$$T_{HS}\approx\frac{\overline{v_{Zp}}}{\overline{v_s}}T_{HP}, \tag{20}$$

since the hohlraum temperature rises linearly with time, and $\overline{v_s}$ is the average shock velocity, including cylindrical or quasispherical convergence. Integrating Eq. (17) we find that

$$\overline{v_s}=\beta_s\overline{v_{Zp}}=\frac{4(1+\mu)}{3}\overline{v_{Zp}}. \tag{21}$$

When the shock arrives at the capsule, the hohlraum temperature will be approximately 60% and 52% of the peak value for cylindrical and spherical pinches, respectively.

If $r_{ab}>r_{cap}$ the incoming shock will be reflected outward. This reflected shock will typically reach the convertor/Z-pinch plasma interface before τ_{cap}, and slow the incoming Z-pinch plasma. Similarly a shock will be reflected from the axis for $|Z|>r_{cap}$. This reflected shock will also propagate outward and slow the incoming Z-pinch plasma, but because of the time delay the Z-pinch plasma will be distorted into a noncylindrical shape as seen in numerical simulations.[5] For simplicity we assume the Z pinch remains cylindrical for our model calculations.

On the other hand, if the shock pressure is larger than the ablation pressure of the capsule, the spherical symmetry of the capsule will be destroyed, unless the initial outer radius of the convertor is large enough so that the capsule is isolated from the shock. This will be true if the initial outer radius of the convertor is approximately

$$r_{co}\approx r_{cap}+\overline{v_s}\tau_{cap}. \tag{22}$$

Note that this is considerably larger than the value given by Eq. (9). The final radius of the interface will be larger by the approximate factor $3/F_s\sim 6$. Therefore, a solid convertor will not work as well as an annular convertor if ablative standoff is not operative.

There is some optimum pinch length for a given capsule and accelerator current that will generate the highest hohlraum temperature. However, our model is not able to find this optimum since the analytic solution for the pinch dynamics does not include the feedback between pinch length and driving current. Therefore, we have simply fixed the length of the pinch at roughly five times the capsule radius, which is the ratio chosen in the high yield design.[5] Detailed numerical simulations indicate that the hohlraum temperature is a weak function of this ratio near this value.

F. Energy balance and radiation transport

The Z-pinch plasma of mass M_Z collides with the convertor of mass M_c. For annular convertors, the shock waves will travel completely through both of these regions on a time scale short compared to the capsule implosion time. The two regions will then be nearly at rest with respect to each other. This is essentially a simple inelastic collision so the energy available to heat the materials and generate radiation is approximately

$$E_A=E_K\left(\frac{M_c}{M_c+M_Z}\right), \tag{23}$$

where E_K is the kinetic energy of the imploding Z-pinch plasma.

One might at first think that we should also use r_{Zib} to compute the kinetic energy, since work is being done by the magnetic field on the Z-pinch plasma after first strike. However, once the initial shock waves have propagated through both the Z-pinch plasma and the convertor the materials are at high pressure and will be difficult to compress further. Thus most of this work will go into kinetic energy, which cannot be converted into radiation until these plasmas stagnate on axis. Thus for annular convertors we shall use r_{co} to calculate the available kinetic energy from Eq. (3).

The situation is more complicated for solid convertors, since the shock can transit the convertor several times. This is because the shock can be reflected from either the capsule ablation surface [as calculated from Eq. (19)] or the axis. For simplicity we will ignore the presence of the capsule. The shock will reflect off the axis and return to the inner radius of the Z-pinch plasma, when it is at the position

$$r_2=\frac{\beta_s-1}{\beta_s+1}r_{co}. \tag{24}$$

At this time the convertor material has been shocked twice. The inward propagating shock drove the convertor material inward at approximately $3\overline{v_{Zp}}/4$. Using the shock relations one can show that the outward shock will bring the velocity of the convertor material back to zero and the energy that remains in the Z-pinch plasma is approximately

$$\left(\frac{M_Z}{M_Z+M_c}\right)^2E_K.$$

When the inner radius of the Z-pinch plasma reaches r_{Zib} the available energy is then given by

$$E_A=\left[1-\left(\frac{M_Z}{M_Z+M_c}\right)^{N_s}\right]E_K, \tag{25}$$

where the shocks have crossed the convertor N_s times with

$$N_s=\frac{2\ln\left(\frac{r_{Zib}}{r_{co}}\right)}{\ln\left(\frac{\beta_s-1}{\beta_s+1}\right)}. \tag{26}$$

This expression yields an available energy significantly larger than is obtained for the annular convertors. As an example, assuming $M_c=M_Z$, $E_A/E_K=1/2$ for an annular convertor, but E_A/E_K can be greater than 0.8 for a solid convertor.

A portion of this available energy will go to internal energy, while the rest will go into radiation, i.e.,

$$E_A = E_{\text{int}} + E_{\text{rad}}. \tag{27}$$

Since we have chosen a low opacity material for the convertor, the radiation temperature will be nearly spatially constant within the convertor/Z-pinch plasma interface at any point in time. We have defined the hohlraum temperature, $T_H(t)$, to be the average radiation temperature within this region. In contrast, the radiation temperature will have significant spatial variation within the Z-pinch plasma due to the high opacity of this material. Let R_{ZH} be the ratio of the spatial average of the radiation temperature in the Z-pinch plasma as compared to T_{HP} the hohlraum temperature. To find R_{ZH} we need to solve the radiation transport to obtain the radiation temperature profile. Since the electron temperature is approximately equal to the radiation temperature, the total internal energy is given by

$$E_{\text{int}} = E_{\text{Z}}(R_{\text{ZH}}T_{\text{HP}})M_{\text{Z}} + E_c(T_{\text{HP}})M_c, \tag{28}$$

where E_Z and E_c are the internal energy functions for the Z-pinch plasma material and the convertor material. We approximate these functions with power law fits to data in the Sesame Equation of State package.[12] Assuming tungsten for the Z-pinch material we obtain

$$E_{\text{Z}}(T) = 7.0\times 10^6 T_{\text{eV}}^{1.35}\rho^{-0.15}\ \text{J/kg}, \tag{29}$$

where T_{eV} is the temperature in units of eV, and ρ is in g/cm^3. Assuming CH_2 for the convertor the energy function is

$$E_c(T) = 2.4\times 10^8 T_{\text{eV}}^{0.88}\ \text{J/kg}. \tag{30}$$

The energy that goes into radiation is composed of three parts

$$E_{\text{rad}} = E_{\text{cap}} + E_w + E_s, \tag{31}$$

where E_{cap} is the energy absorbed by the capsule, E_w is the energy absorbed by the electrode walls, and E_s is the energy radiated from the outer surface of the Z-pinch plasma. These energies depend on the hohlraum temperature and the geometry which are both a function of time. To simplify the model calculations, we wish to relate these energies to the peak hohlraum temperature, T_{HP}, and the initial geometric configuration. The radiation absorbed by the ICF capsule is given by

$$E_{\text{cap}} = (1-\alpha_c)4\pi\sigma\int_0^{\tau_b} r_c^2(t)T_H^4(t)dt \equiv (1-\alpha_c)4\pi\sigma r_{\text{cap}}^2 T_{\text{HP}}^4\tau_{\text{rc}}, \tag{32}$$

where τ_b is the capsule bang time, α_c is the effective albedo of the capsule, $r_c(t)$ is the capsule radius as a function of time, $T_H(t)$ is the hohlraum temperature as a function of time, and r_{cap} is the initial capsule radius. The second and third terms define the effective capsule radiation absorption time, τ_{rc}. For solid convertors, $\tau_b = \tau_{\text{cap}}$, but for annular convertors, $\tau_b = \tau_{\text{cap}} + \tau_r$. Since the outer material of the capsule is chosen to effectively absorb radiation the albedo is low. We use the value of 0.3, which is consistent with typical plastic ablator materials.

A portion of the electrode walls will be exposed to the hohlraum radiation ($r < r_{\text{Zi}}$) as shown in Fig. 2. The radiation lost to the electrodes is given by

$$E_w = (1-\alpha_w)2\pi\sigma\int_0^{\tau_b} r_{\text{Zi}}^2(t)T_H^4(t)dt \equiv (1-\alpha_w)2\pi r_{\text{co}}^2\sigma T_{\text{HP}}^4\tau_{\text{rw}}, \tag{33}$$

where $\alpha_w = 0.8$ is the albedo of the electrode wall, $r_{\text{Zi}}(t)$ is the radius of the interface between the Z-pinch plasma and the convertor as a function of time, and r_{co} is the initial outer radius of the convertor. The second and third terms define the effective time, τ_{rw}, for radiation to be absorbed by the electrode walls.

The radiation lost from the outer surface of the Z-pinch plasma, E_s, is given by the

$$E_s = 4\pi L_{\text{Z}}\sigma\int_0^{\tau_b} T_o^4(t)r_{\text{Zo}}(t)dt \equiv 4\pi r_{\text{Zob}}L_{\text{Z}}\sigma T_{\text{ob}}^4\tau_{\text{rs}}, \tag{34}$$

where $r_{\text{Zo}}(t)$ is the outer radius of the Z-pinch plasma from the time of first strike and $T_o(t)$ is the outer radiation temperature of the Z-pinch plasma. Note the solution for the flux from a plane photosphere[10] is $F = 2\sigma T_{\text{ob}}^4$, where $T_{\text{ob}} = T_o(\tau_b)$. The factor of 2 is due to the increase in temperature going inward from the outer boundary. This factor of 2 is included in the third term which combined with the second term used to define τ_{rs}. The radiation temperature at the outer boundary of the Z-pinch plasma can be determined as a function of the radiation temperature within the hohlraum by solving the radiation transport through the Z-pinch material ($r_{\text{Zi}} < r < r_{\text{Zo}}$). Since the Z-pinch material is highly opaque we use the radiation diffusion approximation. Details are given in Appendix B.

G. The Rayleigh–Taylor instability

The Z-pinch plasma will suffer disruption from the Rayleigh–Taylor (RT) instability as the plasma is imploded. This will decrease the effective opacity of this region, since there will be regions that are much thinner than the average, see Fig. 8(a). The model[13] of Desjarlais and Marder indicates that approximately 90% of the Z-pinch plasma material will be in the Taylor spikes. We shall use the shape shown in Fig. 10 where the curve is assumed to be quadratic. Thus the overall thickness is $\Gamma = \Gamma_{\text{min}} + az^2$ where the constant can be determined from the ratio of the spike/bubble mass, R. The result is $\Gamma = \Gamma_{\text{min}}(1+3Rx^2)$, where $x = 2z/\lambda$. Since radiation transport depends on the Rosseland opacity we want to find the mean

$$\frac{1}{\Gamma_{\text{Ross}}} = \frac{1}{\Gamma_{\text{min}}}\int_0^1 \frac{dx}{1+3Rx^2} = \frac{\tan^{-1}\sqrt{3R}}{\Gamma_{\text{min}}\sqrt{3R}}. \tag{35}$$

For $R = 9$ we obtain $\Gamma_{\text{Ross}} = 3.76\Gamma_{\text{min}}$. Since 90% of the mass is in the spikes for $R = 9$, the thickness would be $10\Gamma_{\text{min}}$ without instabilities. Thus we shall multiply the opacity of the Z-pinch plasma by the factor, $F_{\text{op}} = 0.376$, to take into

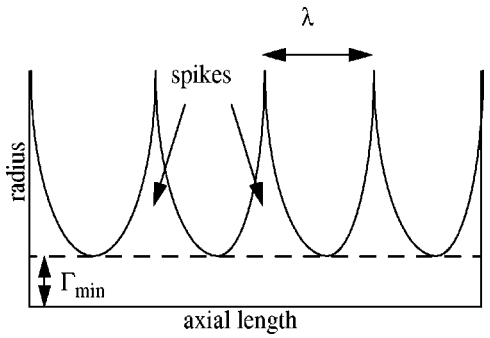

FIG. 10. Schematic of Z-pinch plasma deformed by the RT instability just before striking the convertor.

account the reduced radiation trapping that results from the RT instability. As we show in Sec. V, this leads to a reduction in the peak hohlraum temperature by approximately 20 eV.

H. Numerical procedure

The numerical procedure for using the model equations presented in this section to obtain the peak hohlraum temperature is outlined in this section. The first step is to define various physical quantities that establish a specific dynamic hohlraum setup. These parameters include; I_p, the peak current (typically 20–60 MA); t_r, the rise time to peak current (typically 100 ns); α_c and α_w, the capsule and electrode wall albedos; F_s, symmetry factor ($r_{\mathrm{Zib}}/r_{\mathrm{cap}}$); r_{cap}, the initial capsule radius; r_{Z0}, the initial radius of the Z pinch; L_{Z}, the length of the pinch (typically $5r_{\mathrm{cap}}$); v_f, the final capsule implosion velocity (typically 35 cm/μs); d_{Z}, the thickness of the Z-pinch plasma when it first strikes the convertor ($\sim$2 mm); M_c/M_{Z}, the ratio of the convertor over the Z-pinch masses.

At this point we make an initial guess at the peak hohlraum temperature, T_{HP}. We generate a numerical function of the hohlraum temperature, which will be zero for the correct temperature. The capsule implosion time is determined by Eq. (6) for an annular convertor or Eq. (7) for a solid convertor. The radius of the inner surface of the Z-pinch plasma, at capsule bang time, is determined from F_s and the initial capsule radius. The outer radius of the Z-pinch plasma at capsule bang time, r_{Zob}, is given by the expression $r_{\mathrm{Zob}} = r_{\mathrm{Zib}} + d_{\mathrm{Z}}/4$ where we have assumed the Z-pinch plasma has been compressed by a factor of 4 due to the strong shock produced by the collision with the convertor. The mass of the Z-pinch plasma is determined from Eq. (A6), where $\alpha=0$ for a cylindrical pinch and $\alpha=1/3$ for a quasispherical pinch. The convertor mass is then determined by the ratio M_c/M_{Z}. The average velocity of the inner surface of the Z-pinch plasma, $\bar{v}_{\mathrm{Zp}}$, can be calculated from Eqs. (A8) and (13) for a cylindrical pinch and Eq. (15) for a quasispherical pinch. The initial outer radius of the convertor, r_{co}, is then determined by Eq. (9). The average shock velocity is then found from Eq. (21). The kinetic energy of the pinch, E_K, is found from Eq. (A7). The energy available to heat the materials, E_A, is found from Eq. (23) for annular convertors. Otherwise for solid convertors, Eqs. (25) and (26) must be used to find the available energy and we must solve for r_{ab}/r_c, using Eqs. (17) and (19). The available energy will be divided into the internal energy of the convertor and Z-pinch materials and to radiation. The internal energy is determined by Eq. (28). This result depends on the ratio, R_{ZH}. The temperature profile within the Z-pinch plasma is determined from Eq. (B9) (for cylindrical pinches) or from Eq. (B10) (for quasispherical pinches), where the opacity is determined by Eq. (B7) multiplied by F_{op} to account for the decreased mean thickness of the Z-pinch plasma which results from the RT instability. The radiation absorbed by the capsule is determined by Eq. (32) and the radiation absorbed by the electrode wall is determined by Eq. (33). The remaining energy must be radiated from the outer surface of the Z-pinch plasma. This energy, E_s, defines the radiation temperature, T_o, at the outer surface of the Z pinch at bang time through Eq. (34), and also the specific energy deposition rate through Eqs. (B4) and (B3). Setting $r=r_{\mathrm{Zi}}$ in Eq. (B9) (cylindrical) or Eq. (B10) (quasispherical) we can solve for the hohlraum temperature to obtain a new value, $\tilde{T}_{\mathrm{HP}}$. We define the numerical function as the difference between our original guess and this new value. The root of this function is found using the method of bisection.

III. MODEL RESULTS COMPARED TO EXPERIMENTS

A number of experiments have been performed on the Z accelerator to study the behavior of the dynamic hohlraum.[14] In this section we shall compare our model calculations to some of these dynamic hohlraum experiments. These comparisons are made for the purpose of benchmarking the model so that we can have some confidence in model calculations using drive currents that are not presently accessible to experiment.

A. Foam convertor experiments

Experiments have been performed on the Z accelerator using solid cylindrical convertors composed of low density plastic foam. On shot 291, the outer foam radius was 4 mm with a density of 6 mg/cc. A current pulse rising to approximately 20 MA in 100 ns was delivered to a 1-cm-long array of 240 wires at initial radius of 2 cm. An inner array of 120 wires was located at a radius of 1 cm. The presence of the inner ''nested'' array reduces the effect of the RT instability on the Z-pinch implosion.[15] The wires had a diameter of 7.5 μm and were composed of tungsten. The total mass of the outer array was 2 mg, while the inner array had a mass of 1 mg. The combined mass of the two wire arrays was approximately equal to the mass of the convertor. The radiation temperature was measured by a set of x-ray diodes, bolometers, and time-resolved x-ray pinhole cameras.[16] The hohlraum radiation temperature is plotted (diamonds) as a function of time in Fig. 7.

To model these experiments we assume a single wire array of mass 3 mg at an initial radius of 1.73 cm, which is the mass weighted mean of the nested arrays. The incoming Z-pinch plasma was assumed to be 2 mm thick when it first makes contact with the convertor. This thickness is roughly consistent with the radiation pulse widths that have been

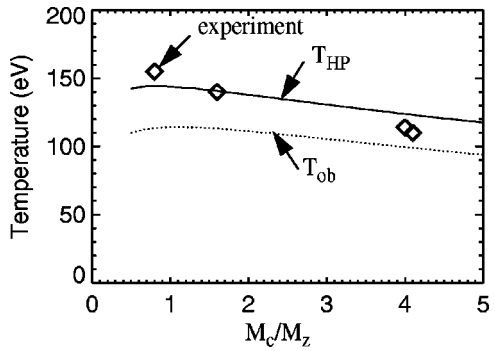

FIG. 11. Hohlraum temperature as a function of the ratio of the convertor to Z-pinch mass M_c/M_Z for annular copper convertors. The results of the model calculations are labeled T_{HP} for the peak hohlraum temperature and T_{ob} for the temperature at the outside of the Z-pinch plasma. The diamonds are experimental measurements of the hohlraum temperature.

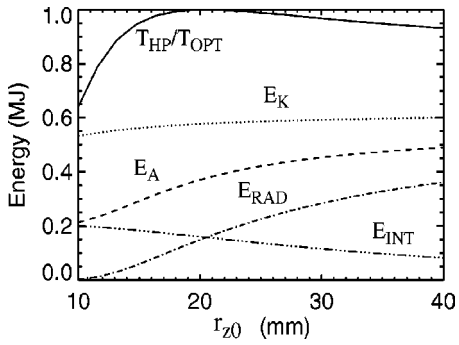

FIG. 12. Normalized hohlraum temperatures (T_{HP}/T_{opt}) as a function of the initial Z-pinch plasma radius for annular 2-mm-thick plastic foam convertors. The mass ratio M_c/M_Z is optimized for each value of r_{Z0}. The available energy (E_A), radiated energy (E_{rad}), and internal energy (E_{int}) are also plotted.

observed[15] in nested wire array pinches that are allowed to stagnate on axis. The model calculations are plotted as a solid line in Fig. 7. As can been seen the agreement between the model and the experiments is quite good.

B. Copper mass scan

An inertial fusion capsule could be imbedded in a solid foam convertor as was studied in the Sec. III A. However, the initial low temperature ($T_{rad}\sim 100$ eV) radiation wave needed to set the capsule implosion on a proper adiabat can arrive at the capsule equator significantly before it arrives at the poles. This is because the radiation wave travels at much less than the speed of light even in a low density plastic foam. This timing difference would result in an asymmetric implosion, without some design mitigation such as a quasi-spherical pinch. The arrival asynchrony could be substantially reduced by using annular convertors, since the radiation wave would then move at the speed of light. Such an annular convertor must have an initial radius large enough so that the capsule implodes before the convertor collapses on the capsule. Initial model calculations and detailed numerical simulations suggest that the hohlraum temperature should be a weak function of the ratio of the convertor mass over the Z-pinch plasma mass and that increasing this ratio should delay stagnation on axis. This would allow a smaller initial radius of the convertor and thus a higher hohlraum temperature.

A series of dynamic hohlraum experiments were performed on the Z accelerator to test this hypothesis. Four shots were performed using the nested wire array configuration described in Sec. III A. The convertor consisted of a 1-cm-long copper tube with a 2.5 mm radius. The wall thickness was different for each shot to provide a scan in the ratio of the convertor to Z-pinch mass. The wall thicknesses were 1.8, 3.7, 9.2, and 9.4 μm, with the corresponding ratios $M_c/M_{ZP}=0.8$, 1.6, 4.0, and 4.1. The hohlraum temperature was determined by measuring x rays through a 2 mm radius aperture on one end of the dynamic hohlraums. The results are shown in Fig. 11 as plots of hohlraum temperature as a function of M_c/M_Z. These data (diamonds) are compared to calculated temperatures using our model (solid line). The agreement is pretty good for small mass ratios; however, the data exhibit a somewhat stronger dependence on the mass ratio than predicted by the model. This may be due to the opacity of copper, which has not been included in the model. An optimum convertor should be of a low opacity material such as plastic.

IV. MODEL RESULTS COMPARED TO DETAILED NUMERICAL SIMULATIONS

The model equations described in Sec. II are easy to solve numerically. An important benefit of such a computationally simple model is that it is easy to obtain many solutions and thus uncover various trends. In Sec. III we obtained the hohlraum temperature as a function of the ratio of the convertor/Z-pinch mass, M_c/M_Z for copper convertors, see Fig. 11. Notice that the hohlraum temperature is a weak function of the mass ratio. This is because increasing the convertor mass extracts more energy from the inelastic collision [see Eq. (23)], but more energy goes into internal energy.

We shall now look at the variations with respect to the initial radius of the Z-pinch plasma. The convertor is still assumed to be a thin (2-mm-thick) annulus, but composed of a fairly dense plastic foam, which has less opacity than copper. For each value of the initial radius of the Z-pinch plasma, the mass ratio M_c/M_Z is optimized to obtain the highest hohlraum temperature. The resulting hohlraum temperature (normalized to $T_{opt}=134$ eV) is plotted in Fig. 12 as a function of the initial radius of the Z pinch, r_{Z0}. In this example the capsule radius is 1 mm, the drive current rises to 20 MA in 100 ns, the Z-pinch plasma is 2 mm thick just prior to first strike, and $F_s=r_{Zib}/r_{cap}=2$. The initial convertor radius determined by Eqs. (9) and (15) is found to be approximately 5 mm. Notice that the hohlraum temperature is a fairly strong function of the initial Z-pinch plasma radius for values below optimum. This is because small initial radii require large Z-pinch plasma masses to maintain the correct implosion time and thus most of the kinetic energy goes into internal energy rather than radiation. The function is weak for initial radii greater than optimum because the reduction in mass is compensated by the increase in the radiation lost,

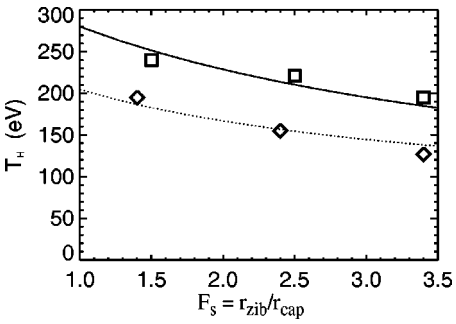

FIG. 13. Hohlraum temperature as a function of $F_s = r_{\mathrm{Zib}}/r_{\mathrm{cap}}$ for annular 2-mm-thick foam convertors. The dotted curve corresponds to performance of the existing Z-accelerator ($I_p = 20$ MA, $r_{\mathrm{cap}} = 1$ mm). The diamonds are the result of numerical simulations for the optimized parameters obtained from the model. The solid curve corresponds to an advanced accelerator ($I_p = 60$ MA, $r_{\mathrm{cap}} = 2$ mm). The squares are the results of numerical simulations for these optimized parameters.

since the degree of radiation trapping is reduced. However, this weak behavior probably does not continue for arbitrarily large initial wire radius, due to the RT instability. One would expect that a RT bubble would break through the Z-pinch plasma if the initial radius is too large. Furthermore, the optical depth of the Z-pinch plasma is less than unity for the large initial radii so the diffusion approximation is no longer valid. Fortunately, this is clearly not the region of interest.

In our next example, the symmetry factor, F_s, is varied, while the initial radius and the mass ratio M_c/M_{Z} are both optimized. The results are shown in Fig. 13. Two curves are plotted. Parameters corresponding to the performance that can be expected from the existing Z-accelerator were used for the dotted curve. Here the current rises to a peak value of 20 MA in 100 ns and the capsule radius is 1 mm. The model indicates that $r_{\mathrm{Z0}} = 2$ cm, $M_c/M_{\mathrm{Z}} = 2$, and $M_{\mathrm{Z}}/L_{\mathrm{Z}} = 3$ mg/cm are near optimum. Parameters corresponding to the performance that could be expected from an advanced accelerator were used to generate the solid curve. Here the current rises to 60 MA in 100 ns and the capsule radius is assumed to be 2 mm. Optimum parameters are found to be; $r_{\mathrm{Z0}} = 3$ cm, $M_c/M_{\mathrm{Z}} = 3$, $M_{\mathrm{Z}}/L_{\mathrm{Z}} = 15$ mg/cm. We have omitted the correction for the RT instability, F_{op}, so that these results could be directly compared to 1-D numerical simulations using a detailed radiation hydrodynamics code.[9] The optimized values of the initial radius, Z-pinch mass, and the convertor mass were used to set up these simulations. The convertor was chosen to be CH plastic foam, with an initial inner radius set to r_{Zib}, and an initial outer radius determined by Eq. (9). A thin layer of gold (0.4 μm) on the outside of the convertor was found to reduce the ablation in response to the roughly 30 eV radiation generated in the Z-pinch plasma during the implosion phase. The Z-pinch plasma (tungsten) was initiated with a thickness of 1 mm as an approximation to the conditions expected after the wire array undergoes the initial ohmic heating. An external circuit was used to generate the Z-pinch current with lumped circuit elements ($R \sim 1/8\,\Omega$, $L = 12$ nH) and a time-dependent voltage. The implosions occurred at about 135 ns. Absorption of radiation by the capsule was simulated by a radiation leak of the same surface area as each respective capsule. The average hohlraum temperatures over the capsule implosion time obtained from the simulations are plotted as diamonds for *Z* parameters and as squares for *X* parameters. As can be seen there is good agreement between these simulations and the model calculations. This illustrates the usefulness of such a computationally simple model, since performing the double optimization with a detailed simulation code would take a long time. The results of Fig. 13 indicate that decreasing the value of F_s substantially increases the hohlraum temperatures. However, the simulations show that the convertor will be driven into the capsule before it is fully imploded if F_s is too small. The numerical simulations indicate that F_s must be greater than 1.5 to hydrodynamically isolate the capsule. This would limit the peak hohlraum temperature to approximately 230 eV, when the effect of the RT instability is included, even with a 60 MA drive current. Smaller values of F_s and hence higher temperatures are possible using solid foam convertors because of ablative standoff as described in Sec. II E.

V. SCALING RESULTS

A. Ablative standoff

A low density solid foam convertor has two important advantages over annular convertors. First, the fraction of the collision energy that goes into shock heating the Z-pinch plasma decreases as the convertor density is decreased, [see Eq. (B4)]. This will decrease the outward radiation losses and result in higher hohlraum temperatures. Second, the transit time of the shock through the convertor can be as long as the implosion time of the capsule. This continuous heating can result in a rising hohlraum temperature during the capsule implosion. Proper density profiling of the convertor should result in ''pulse shaping'' which can drive an isentropic implosion. In fact, numerical simulations[5] indicate that a nearly isentropic implosion results without any density profiling. Furthermore, these simulations indicate that the Z-pinch plasma/convertor does not crush the capsule even though the radius of the interface is less than the original capsule radius at the time of the capsule implosion, i.e., $F_s < 1$. This is in spite of the fact that near the electrodes a shock wave has been driven all the way to the axis before the capsule implosion. The shock wave does not destroy the symmetry of the capsule due to ablative standoff. The shock is isolated from the imploding portion of the capsule by the outward moving material that has been ablated from the capsule by the hohlraum radiation field. This ablative standoff only occurs if the ablation ram pressure is larger than the shock pressure. The equations describing this process are given in Sec. II E. The general requirements are high radiation temperatures and low convertor densities. Since the capsule symmetry is not adversely affected by the incoming shock, ablative standoff allows small values of F_s, which implies higher hohlraum radiation temperatures. This is true for several reasons. More Z-pinch kinetic energy is available when the pinch is driven to a smaller final radius. Less radiation is lost because of the smaller final radius. Furthermore, the incoming shock will be reflected from both the axis and the capsule ablation material. This outward reflected

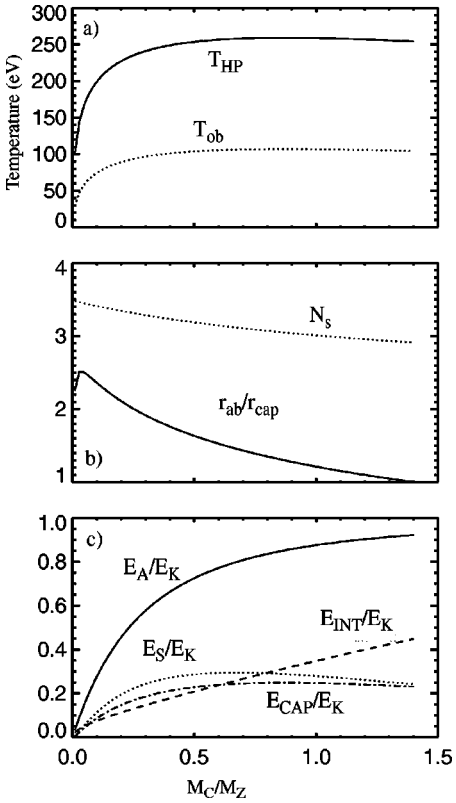

FIG. 14. Results from model calculations assuming a solid foam convertor with a peak drive current of 55 MA, a Z-pinch mass of 48 mg, an initial Z-pinch radius of 1.8 cm, a Z-pinch kinetic energy of 7 MJ; a capsule radius of 2.75 mm, and a symmetry factor $F_s=0.6$. All parameters are plotted as a function of M_c/M_Z. The peak hohlraum temperature, T_{HP}, and outer surface temperature of the convertor, T_{ob}, are plotted in (a). The ratio of the ablation standoff radius, r_{ab}, to the initial capsule radius, r_{cap}, and the number of shocks passing through the convertor, N_s, are plotted in (b). The ratios of the energy available for heating, E_A, the energy lost from the outer surface of the pinch as radiation, E_s, the energy absorbed by the capsule, E_{cap}, and the internal energy, E_{int}, over the kinetic energy of the incoming Z-pinch plasma, E_K, are plotted in (c).

shock will further slow down the incoming convertor and Z-pinch plasma turning this kinetic energy into heat. Since the shock reflection occurs earlier at the capsule equator than elsewhere, the Z-pinch plasma will wrap around the capsule forming a somewhat spherical hohlraum. These effects all conspire to produce a hotter hohlraum than would be produced by an annular convertor.

The results of a model calculation assuming a peak drive current of 55 MA, a rise time of 100 ns, and an initial Z-pinch radius of 1.8 cm are shown in Fig. 14. These parameters are the same as those used in the recent high yield design.[5] The results are plotted as a function of the ratio M_c/M_Z. The peak hohlraum temperature has a maximum of approximately 260 eV for $M_c/M_Z \sim 0.8$. This is substantially below the value of about 300 eV that was observed in detailed numerical simulations of the high yield capsule.[5] However, the numerical simulations did not include the effect of the Rayleigh–Taylor instability and radiation loss to the electrode surfaces. Indeed, removing these effects from our model increases the calculated peak temperature to approximately 290 eV, which is close to the results of the simulations. Improvements have been made to the simulation code that will allow the inclusion of these effects and we plan to revisit these design calculations. It will be interesting to see if the peak temperature is reduced by a significant amount as our model predicts.

The ratio of ablation standoff radius to the capsule radius, r_{ab}/r_{cap}, is a decreasing function of M_c/M_Z, because the initial shock pressure depends on the convertor density. The number of shock transit times, N_s, is approximately three, which means that a second shock will usually reach the capsule before it is fully imploded. This shock will be stronger than the first shock due to the higher convertor density and could possibly damage the symmetry of the capsule. However, the hohlraum temperature will be roughly at its peak value when the second shock arrives and the ablation pressure may still be able to standoff this second shock. We do not think it is practical to include the standoff of the second shock in our simple model. However, the ablation pressure was sufficient to provide standoff of the second shock in the detailed numerical simulations.[5] The energy accounting is shown in Fig 14(c). The kinetic energy of the Z pinch was approximately 7 MJ and is not a function of the ratio M_c/M_Z. However, the energy available for heating rises monotonically with M_c/M_Z. This is the reason for the initial rise in the hohlraum temperature as M_c/M_Z increases. The temperature reaches a maximum and then starts to fall slowly because of the extra mass that must be heated. This can be seen from the behavior of the curve labeled, E_{int}/E_K.

The behavior of the dynamic hohlraum as the initial radius of the Z pinch is varied is shown in Fig. 15, where, $I_p=55\,\mathrm{MA}$, $r_{cap}=2.75\,\mathrm{mm}$, and $F_s=0.6$. The optimum convertor mass is found for each value of the initial radius, r_{Z0}. For small initial radii, an increase in the initial radius increases the hohlraum temperature because the energetics are dominated by the internal energy, E_{int}, which decreases due to the smaller Z-pinch mass. Continuing to increase the initial radii results in too small a Z-pinch mass to effectively trap the radiation. This effect is seen in the functional behavior of the outer temperature of the Z-pinch plasma at capsule bang time, T_{ob}, the optical depth, and the radiation energy lost from the outer surface of the Z-pinch plasma, E_s. The maximum hohlraum temperature occurs for an initial radius of approximately 1.9 cm, which happens to be very close to the value used for the high yield design.

The hohlraum temperature as a function of the drive current for optimized values of the convertor mass and the initial Z-pinch radius is shown in Fig. 16. A capsule the size of the high yield capsule, i.e., $r_{cap}=2.75\,\mathrm{mm}$ has been assumed. The optimum ratio M_c/M_Z is found to be nearly constant at 0.8 so we have not plotted it. The available energy rises as the square of the drive current, but due to the fourth power dependence of the radiation loss the hohlraum temperature rises approximately as the square root of the current. The degree of radiation trapping increases with drive current as seen by the number of optical depths, τ, in the Z-pinch plasma. The fraction of the available energy that is lost to radiation and that is absorbed by the capsule is nearly independent of the drive current. The optimal initial radius of the convertor only increases from 1.2 cm at $I_p=20\,\mathrm{MA}$ to 1.5

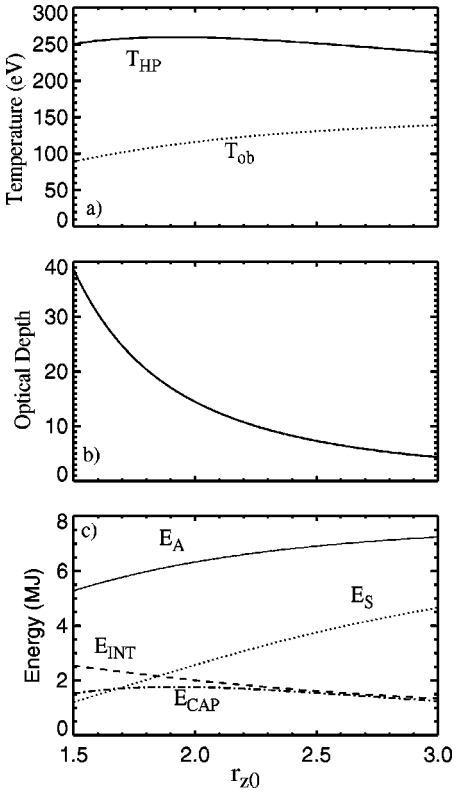

FIG. 15. Results from model calculations assuming a solid foam convertor with a peak drive current of 55 MA, a capsule radius of 2.75 mm, and a symmetry factor $F_{sym}=0.6$. Parameters for optimal convertor mass are plotted as a function of the initial Z-pinch radius, r_{Z0}. The peak hohlraum temperature, T_{HF}, and outer surface temperature of the convertor, T_{ob}, are plotted in (a). The optical depth with the Rayleigh–Taylor factor included is plotted in (b). The energy available for heating, E_A, the energy lost from the outer surface of the pinch as radiation, E_s, the energy absorbed by the capsule, E_{cap}, and the internal energy, E_{int}, are plotted in (c).

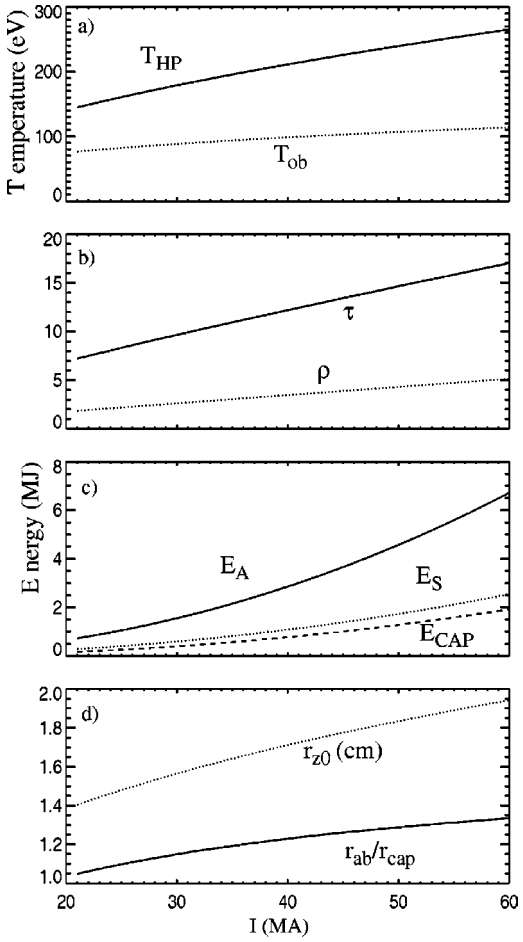

FIG. 16. Optimized results (with respect to both convertor mass and initial Z-pinch radius) are plotted as a function of the peak drive current, I_p. The convertor is solid foam, the capsule has a radius of 2.75 mm, and the symmetry factor $F_s=0.6$. The peak hohlraum temperature, T_{HP}, and outer surface temperature of the convertor, T_{ob}, are plotted in (a). The optical depth with the Rayleigh–Taylor factor included and the optimum foam density (g/cc) are plotted in (b). The energy available for heating, E_A, the energy lost from the outer surface of the pinch as radiation, E_s, and the energy absorbed by the capsule, E_{cap}, are plotted in (c). The optimal initial Z-pinch radius, r_{Z0} (cm) and the ratio of the ablation standoff radius to the capsule radius, r_{ab}/r_{cap} are plotted in (d).

cm at $I_p=60$ MA, but this results in a significant change in the foam density. A foam density of 2 mg/cc is optimal at 20 MA, which is the current that can be produced by the existing Z accelerator. However, the minimum foam density that can be can be produced by the present state of the art is approximately 5 mg/cc, so the optimum design may not be practical at low current drives. Notice also that the ablation standoff radius is nearly the capsule radius at the lower current drives. Reducing the capsule radius to 1.5 mm results in higher radiation temperatures and optimal foam densities ($r_{co}\sim 0.7$ cm) as seen in Fig. 17, but the ablative standoff is still marginal. Clearly detailed numerical simulations and experiments will be needed to determine if ablative standoff can be used with current drives less than about 40 MA.

B. Radiation trapping

A significant uncertainty affecting the performance of the dynamic hohlraum is the degree of radiation trapping that will be achieved by the Z-pinch plasma once it implodes onto the convertor. The computation of the opacity of high Z materials is extremely difficult and thus prone to error. Furthermore, as discussed in Sec. II G, the RT instability will reduce the effective optical depth of the Z-pinch plasma due to the bubble and spike structure. In this section, we explore the sensitivity of the dynamic hohlraum performance to such uncertainties in the degree of radiation trapping. For this study, we have multiplied the opacity in our model calculations by the variable factor F_{op} rather than the fixed factor of 0.37. The results are plotted in Fig. 18. The solid lines are for advanced accelerator performance as would be expected on the proposed *X* machine, i.e., a drive current of 55 MA and a capsule radius of 2.75 mm. The dotted curves are for present day performance that could be expected on the existing Z machine, i.e., a drive current of 20 MA and a capsule radius of 1.5 mm. The results indicate that the hohlraum temperature is reduced by approximately 10–15 eV when $F_{op}=0.37$, which corresponds to the RT corrections that have been made in the previous section. As might be expected the performance falls off faster as F_{op} decreases. As seen in Fig. 18(b), the fraction of the available energy for heating that is lost by radiation increases as F_{op} decreases. This fraction is larger for the Z parameters because the mass of the Z pinch

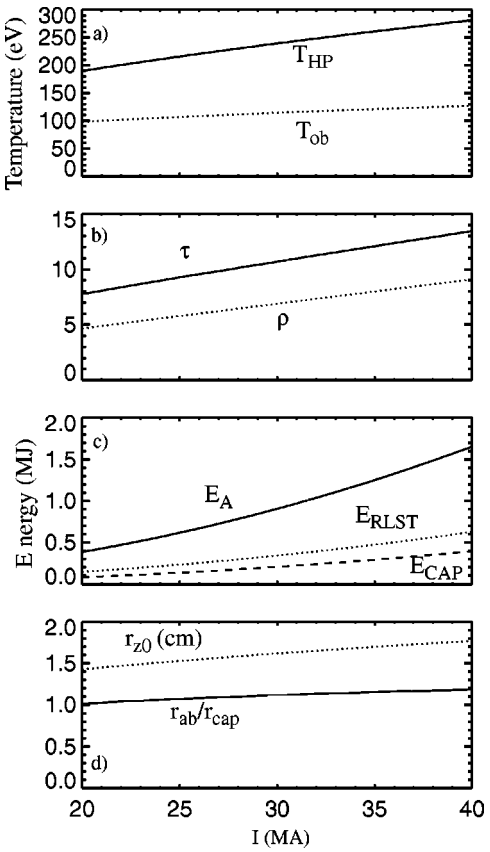

FIG. 17. Same parameters as Fig. 16 but assuming a capsule radius of 1.5 mm.

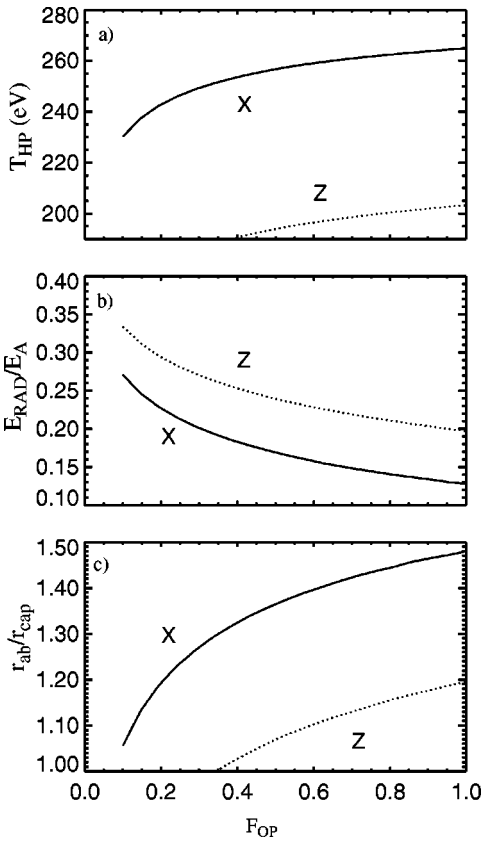

FIG. 18. Optimized results as a function of the opacity multiplier F_{op}, see the text for a description. The solid curves labeled *X* are results assuming a peak drive current of 55 MA and a capsule radius of 2.75 mm. The dotted curves labeled *Z* are results assuming a peak drive current of 20 MA and a capsule radius of 1.5 mm. The hohlraum temperature is plotted in (a), the fraction of the available energy that goes into radiation is plotted in (b), and ratio of the ablative standoff radius to the initial capsule radius is plotted in (c).

is much smaller. The ratio r_{ab}/r_{cap} indicates the strength of the ablative standoff, which is considerably larger for *X* parameters. We assume that ablative standoff will not be effective when $r_{ab}/r_{cap}<1$. It should be noted that stagnation of the Z-pinch plasma against the convertor may increase F_{op} above our estimated value of 0.37 with a significant benefit to the hohlraum performance. It may also be worth using a mixture of elements to create materials with higher opacity than a single element to improve radiation trapping.

C. Quasispherical Z-pinch implosions

An initially cylindrical Z pinch will deform to a quasispherical shape if the Z-pinch material has an appropriate axial mass profile, i.e., heavier at the midplane and lighter at the ends. The determination of the initial mass profile that will provide a quasispherical final configuration can most readily be found by trial and error. Since this could require many iterations, we developed a simple 2-D numerical model of an imploding Z pinch. We assume azimuthal symmetry and represent the Z pinch as a number of particles (actually rings). We assume a fixed current wave form typical of a Z-pinch shot on the existing Z accelerator and calculate the **I×B** force on each of these particles and then move them accordingly. The model ignores the effects of material pressure. Furthermore, the evolution of the pinch can only be simulated until a pair of particles crosses. Thus a relatively small number (10–15) of particles can be used. Despite these limitations, the model has proved to be very useful for finding mass distributions that result in quasispherical final configurations. The results of such a simulation are shown in Fig. 3. The position of particles, marked with a plus sign (+), are shown at various times during the implosion. Initially the pinch was cylindrical with a radius of 2 cm and axial length of 1 cm. The initial mass/length, Λ, is given by Eq. (1). As can be seen the final shape is nearly spherical, which should provide better coupling to the spherical inertial fusion capsule. Similar results have been obtained by others.[7] There are several potential advantages to using a quasispherical Z pinch to drive a dynamic hohlraum. First, the outer surface area of a quasispherical Z pinch is smaller than for a cylindrical pinch, which reduces radiation losses. Second, the areal density of a quasispherical Z pinch is larger than a cylindrical Z pinch of the same mass. This further reduces radiation losses. Third, the nearly spherical final configuration should provide better macroscopic radiation uniformity (not referring to the RT effects discussed earlier).

Detailed numerical simulations will be needed to determine if quasispherical Z-pinch implosions can improve the radiation uniformity, but we have used our model to predict the improvement in hohlraum temperature that results from the first two advantages. The results are shown in Fig. 19. The results indicate an increase of approximately 20 eV

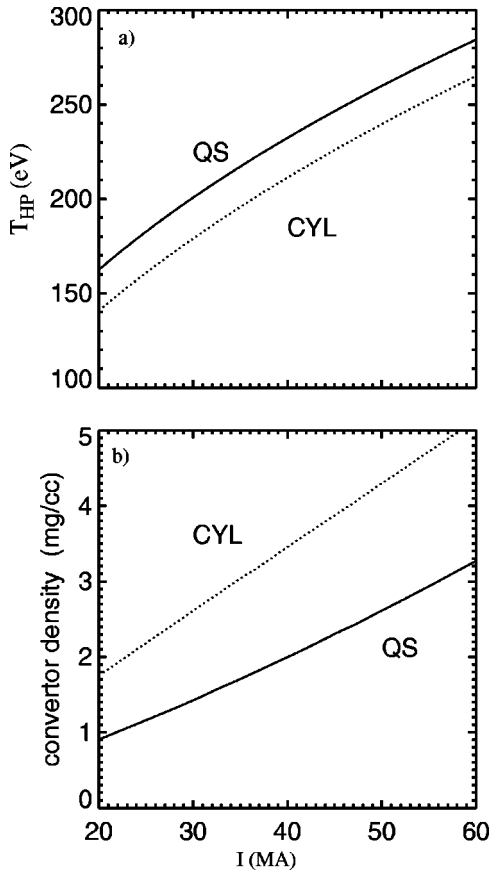

FIG. 19. Comparison between cylindrical (labeled CYL) and quasispherical (labeled QS) dynamic hohlraum model calculations. A capsule radius of 2.75 mm is assumed and $\alpha=1/3$ for the quasispherical calculation. Hohlraum temperatures are plotted in (a) and convertor densities in (b).

nearly independent of the drive current. Although this may not seem like a large improvement, one must remember that the radiation intensity is proportional to the fourth power of the temperature, so this represents an improvement in the radiation intensity of 35% at 60 MA and 75% at 20 MA. Inspection of Fig. 19(b) reveals that the foam density is substantially lower for the quasispherical Z pinches. This is because the initial convertor radii are about the same in either the cylindrical or the quasispherical pinches, but there is greater volume compression in the quasispherical pinches. Presently the lowest foam densities that can be fabricated are approximately 5 mg/cc. To determine the importance of this limitation on the fabrication of foam convertors, we have calculated the hohlraum temperature with the convertor density fixed at 5 mg/cc. The results are shown in Fig. 20. We have chosen a capsule radius of 1.25 mm for these calculations because the model predicts that larger capsules will not exhibit ablative standoff at drive currents as low as 20 MA with this foam density. The results indicate that the temperature increase in a quasispherical pinch is approximately the same even if the foam is higher than optimal, i.e., 5 mg/cc. Of course, the temperatures for both cylindrical and quasispherical are somewhat lower.

We have investigated the behavior of mass profiled Z pinches using the 2-D magnetohydrodynamic code MACH2.[17] This code calculates all three components of the velocity and

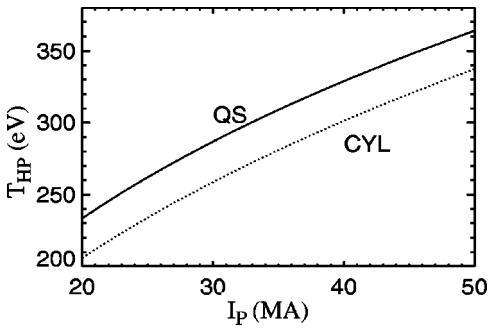

FIG. 20. Comparison between cylindrical and quasispherical dynamic hohlraum temperature model calculations assuming a fixed convertor density of 5 mg/cc. A capsule radius of 1.25 mm is assumed and $\alpha=1/3$ for the quasispherical calculation.

magnetic field vectors on an Arbitrary Lagrangian/Eulerian mesh. The electron, ion, and radiation temperatures are calculated. Generalized Ohm's law and tabular equations of state are used. An important feature of the code is that it can handle complex shapes. Density contours at a time near final collapse for two simulations are shown in Fig. 21. The initial mass/length profiles were calculated using Eq. (1) with $a_2=-0.06$ and $a_4=0.024$. The upper simulation used a mesh size of 156 μm, while the lower simulation used a cell size of 78 μm. Note the clear development of the Rayleigh–Taylor instability even though no random density seed was used in these calculations. In contrast, simulations performed with uniform mass/length and no random seed show no development of instability. The effect of the RT instability is considerably larger for simulations performed with the smaller cell size. We attempted to run simulations with even smaller cell size, but large RT bubble formation caused the simulations to crash early in the implosion. This dependence on the cell resolution may explain why previous low resolution numerical simulations of mass profiled Z pinches[7] did not exhibit Rayleigh–Taylor growth.

These results suggest that obtaining a well-behaved quasispherical Z-pinch implosion by tailoring the mass profile may increase the effect of the RT instability. The magnitude of this effect may be difficult to determine numerically. Considering the potential advantages of quasispherical Z

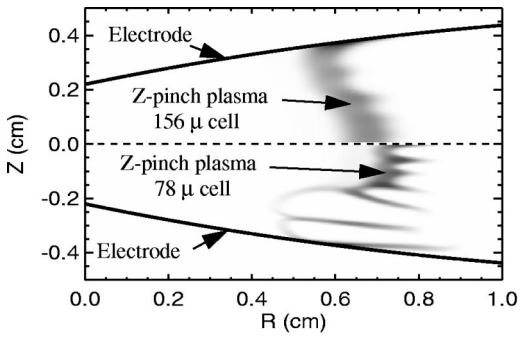

FIG. 21. Contour plots of the Z-pinch plasma density from two different MACH2 simulations using different cell resolutions. The results using 156 μm cells are displayed in the upper half, while the results using 78 μm cells is displayed in the lower half. The initial density profile was the same for both simulations as determined by Eq. (1) with $a_2=-0.06$ and $a_4=0.024$.

pinches, e.g., higher peak hohlraum temperatures, improved radiation symmetry, the approach should be tested experimentally. Such experiments should become practical with the development of the x-ray backlighter on the Z accelerator.

VI. CONCLUSIONS

We have presented a quasianalytic model of the dynamic hohlraum, which includes most of the important physics for determining the hohlraum radiation temperature. The model includes the Z-pinch implosion dynamics, the conversion of the Z-pinch energy into heat and radiation, the loss of radiation to the electrode walls and through the Z-pinch plasma, and radiation absorbed by the capsule. This model has been used to determine the expected performance scaling (peak hohlraum temperature) of the dynamic hohlraum as a function of the many parameters that determine this system. As an example, the model has been used to compute hohlraum temperatures within dynamic hohlraum experiments using a solid foam convertor. The results are in good agreement with the experimental data. Calculations of the peak hohlraum temperature as a function of the ratio of the convertor mass to the Z-pinch mass have also been compared to experimental data. The agreement with this data, which was obtained using annular copper convertors, is not quite as good as for the foam convertors, but still within about 10 eV.

The model has been used to find the optimum values of the ratio of the convertor mass to the Z-pinch mass and the initial Z-pinch radius for annular convertors. Detailed one-dimensional numerical simulations using these optimized values compared well to the results of our model. The results show that the peak hohlraum temperature is a strong function of the radius of the interface between the Z-pinch plasma and the convertor at the capsule implosion time, r_{Zib}. Smaller values result in higher temperatures. We have presented view factor calculations indicating that adequate radiation symmetry can be obtained despite the RT instability if this interface radius is always at least twice the radius of the imploding capsule. This condition is satisfied if the symmetry factor, $F_s = r_{\mathrm{Zib}}/r_{\mathrm{cap}} > 0.5$, where r_{cap} is the initial radius of the capsule. Small values of F_s lead to high peak hohlraum temperatures, which are suitable for driving fusion capsules. If radiation temperature variations induced by the RT instability are larger (>30%) or the wavelengths longer (~1 mm) than indicated by the numerical simulations, the symmetry factor will need to be larger, with an associated decrease in the peak hohlraum temperature. Therefore, the determination of the wavelength and amplitude of the radiation source variations produced within the convertor by the RT instability is of critical importance toward determining if the dynamic hohlraum concept is a viable approach to inertial confinement fusion. Experiments are planned to determine both the wavelength and the radiation temperature variations induced by the RT instability. Note that means for eliminating the radiation asymmetry caused by the cold end electrodes, such as quasispherical implosions, must also be explored.

We have used the model to investigate dynamic hohlraum performance using a solid foam convertor, which has been used in a recent high yield design.[5] Numerical simulations of the high yield design show a phenomenon that we call ''ablative standoff.'' The inward shock wave generated by the Z-pinch plasma colliding with the foam convertor does not penetrate to the inside of the capsule because of the outward motion of the radiatively ablated material. We have calculated the radius of the standoff point as a function of drive current and capsule size. We find that ablative standoff works well at the high current drives needed for a high yield capsule, but not as well at the lower current drives that are presently available. Thus it may be difficult to demonstrate this phenomenon without an upgrade to the existing accelerator.

Scaling of the hohlraum temperature with the degree of radiation trapping has been determined using the model. The results indicate that a decrease in the effective optical depth of the Z-pinch plasma by a factor of 2 results in a decrease of about 10 eV in the peak hohlraum temperature. The degree of trapping might be improved by using a mixture of elements to increase the opacity. This would be most beneficial for demonstrating ablative standoff with relatively low current drives.

A quasispherical Z-pinch implosion develops if the initial Z pinch has an appropriate mass profile. The final shape near stagnation can be nearly spherical (quasispherical). We have used the model to estimate the performance advantage of quasispherical Z pinches over purely cylindrical pinches. The results indicate that the quasispherical dynamic hohlraum should reach a temperature of roughly 20 eV higher than a purely cylindrical pinch. This result is nearly independent of the drive current. Unfortunately, numerical simulations indicate that the mass profile needed to produce a quasispherical Z-pinch implosion also provides a seed for the Rayleigh–Taylor instability. Experiments should be performed to determine if this approach can be made to work.

ACKNOWLEDGMENTS

We wish to thank Thomas Mehlhorn for helpful discussions and encouragement during the course of this work and Mike Desjarlais for comments on the manuscript. We thank Paul Mix for help with the graphics and also acknowledge the technical help of the Z-crew. This work performed at Sandia National Laboratories. Sandia is a multiprogram laboratory operated by Sandia Corporation, a Lockheed Martin Company, for the United States Department of Energy under Contract No. DE-AC04-94AL85000.

APPENDIX A: ANALYTIC Z-PINCH SOLUTION

Analytic solutions for cylindrical and quasispherical Z pinches are derived in this Appendix. The equation of motion for a cylindrical Z pinch is given by

$$M_{\mathrm{Z}} \frac{d^2 r_{\mathrm{Z}}}{dt^2} = -\frac{B^2}{2\mu_0} A_{\mathrm{Z}}(r_{\mathrm{Z}}), \tag{A1}$$

where M_{Z} is the total mass of the Z-pinch plasma, r_{Z} is the radius of the pinch, B is the strength of the B field produced by the Z current, $B = \mu_0 I/2\pi r$. To include quasispherical Z-pinch implosions we use the expression for the area

$$A_Z(r_Z)=2\pi r_Z L_Z\left(\frac{r_Z}{r_{Z0}}\right)^{\alpha}, \tag{A2}$$

where L_Z is the length of the pinch, $\alpha=0$ corresponds to cylindrical convergence, and $\alpha=1/3$ corresponds to the quasispherical pinch depicted in Fig. 3. A solution to Eq. (A1) is found by using the trial solution

$$r_Z=r_{Z0}\left(1-\left(\frac{t}{t_p}\right)^{\beta}\right)^{\zeta}, \tag{A3}$$

where t_p is the time to stagnation. Substitution into Eq. (A1) reveals that the choice $\beta=4$, and $\zeta=1$ yields a solution with a drive current that rises linearly with time as is typically observed in the experiments. The result is

$$I^2=I_p^2 h(\alpha)\left(\frac{t}{t_p}\right)^2\left(1-\left(\frac{t}{t_p}\right)^4\right)^{1-\alpha}, \tag{A4}$$

$$r_Z=r_{Z0}\left(1-\left(\frac{t}{t_p}\right)^4\right), \tag{A5}$$

where I_p is the peak current, and

$$h(\alpha)=\frac{(3-2\alpha)^{3/2-\alpha}}{(2-2\alpha)^{1-\alpha}}.$$

The normalized drive current and Z-pinch radius for a cylindrical pinch ($\alpha=0$) are shown in Fig. 4. The rise time to peak current is $t_r=t_p/(3-2\alpha)^{1/4}$, the pinch mass/length is

$$\frac{M_Z}{L_Z}=f(\alpha)\left(\frac{\mu_0}{4\pi}\right)\left(\frac{I_p t_r}{r_{Z0}}\right)^2, \tag{A6}$$

where

$$f(\alpha)=\frac{(3-2\alpha)^{2-\alpha}}{12(2-2\alpha)^{1-\alpha}}.$$

The kinetic energy of the pinch is

$$E_K=g(\alpha)L_Z\left(\frac{\mu_0}{4\pi}\right)I_p^2\left(1-\frac{r}{r_{Z0}}\right)^{3/2}, \tag{A7}$$

where

$$g(\alpha)=\frac{2(3-2\alpha)^{3/2-\alpha}}{3(2-2\alpha)^{1-\alpha}}.$$

The velocity of the pinch can be found easily from Eq. (A5). The result is

$$v_{Zp}(r_Z)=\frac{4r_{Z0}}{t_p}\left(1-\frac{r_Z}{r_{Z0}}\right)^{3/4}. \tag{A8}$$

We have compared the analytic solution for the kinetic energy of the pinch to a numerical solution with lumped circuit elements which approximates the current provided by the Z accelerator. The voltage is assumed to be of the form

$$V=5.5\sin\left(\frac{\pi t}{2t_r}\right)\mathrm{MV},$$

which drives current through a series inductance of 11.4 nH and resistance of 0.12 Ω. The result of this comparison is shown in Fig. 5. The agreement is very good up to a convergence ratio of approximately 10. Since the dynamic hohlraum stagnates on a convertor the convergence ratio (~4) is substantially less than 10 and the analytic solution should not introduce significant error.

APPENDIX B: RADIATION TRANSPORT SOLUTION

The Z-pinch plasma is of high opacity so that it can effectively trap the radiation. Therefore the diffusion approximation is appropriate with the radiation flux given by

$$F=-\frac{4\sigma}{3\kappa\rho}\frac{d}{dr}T_R^4, \tag{B1}$$

where σ is the Stefan–Boltzmann constant, κ is the opacity, T_R is the radiation temperature, and ρ is the density. In steady state energy conservation yields

$$\nabla\cdot\mathbf{F}=\epsilon. \tag{B2}$$

The specific power, ϵ, deposited in the Z-pinch plasma is given approximately by

$$\epsilon=\frac{f_Z(E_A-E_{\mathrm{int}})}{V_Z\tau_{\mathrm{rs}}}, \tag{B3}$$

where V_Z is the volume of the Z-pinch plasma, E_A given by Eq. (23) for annular convertors or Eq. (25) for solid convertors, E_{int} is given by Eq. (28), and f_Z is the fraction of the shock heating that goes into the Z-pinch plasma. Note that we assume the fraction of the shock energy that goes into radiation will be approximately the same in both regions, so that f_Z is also the fraction of the radiated energy that is emitted by the Z-pinch plasma. We estimate the fraction of shock heating from the following argument. In the center of mass frame for the collision, two stagnation shocks will propagate away from the initial point of contact. The material between these shocks will have little relative motion, so the pressure must be nearly constant in these regions. When the shocks have traveled through both materials the pressure will be approximately the same in both regions. Since pressure is approximately proportional to the material energy density (exactly true for an ideal gas), the fraction of the energy that goes into the Z-pinch plasma will be roughly proportional to the ratio of the volume of the Z-pinch plasma over the total volume of the Z-pinch plasma and the convertor. We assume that the shocks are strong so the density has increased in both regions by about a factor of 4 so we can use the initial volumes at the point of contact. Thus we obtain

$$f_Z\sim\frac{V_Z}{V_c+V_Z}, \tag{B4}$$

where V_c is the volume of the convertor and V_Z is the volume of the Z-pinch plasma at first contact. For cylindrical geometry $V_Z=\pi(r_{Zob}^2-r_{Zib}^2)L_Z$ and $V_c=\pi(r_{co}^2-r_{ci}^2)L_Z$, while for quasispherical geometry $V_Z=\frac{4}{3}\pi(r_{Zob}^3-r_{Zib}^3)$ and $V_c=\frac{4}{3}\pi(r_{co}^3-r_{ci}^3)$. We shall assume that ϵ is constant and thus Eq. (B2) can be integrated.

The radiation flux within the Z-pinch plasma for cylindrical geometry is

$$F=\frac{\epsilon r}{2}+\frac{1}{r}\left(\frac{E_s}{2\pi L_Z \tau_{rs}}-\frac{\epsilon r_{Zob}^2}{2}\right), \tag{B5}$$

where the condition $F(r_{Zob})2\pi r_{Zob}L_Z=E_s/\tau_{rs}$ has been used to determine the constant of integration.

The radiation flux for spherical geometry is

$$F=\frac{\epsilon r}{3}+\frac{1}{r^2}\left(\frac{E_s}{4\pi\tau_{rs}}-\frac{\epsilon r_{Zob}^3}{3}\right), \tag{B6}$$

where the condition $F(r_{Zob})4\pi r_{Zob}^2=E_s/\tau_{rs}$ has been used to determine the constant of integration.

Lindl[8] gives the power law fit to the opacity of gold

$$\kappa=\kappa_0 T_{heV}^{-\beta}\rho^{0.3}, \tag{B7}$$

where $\beta=1.5$, $\kappa_0=6\times10^3\ \mathrm{cm^2/g}$, and T_{heV} is the temperature in units of 100 eV. This should be a reasonably good approximation for the opacity of tungsten. Using this relation Eq. (B1) can be put in the form

$$F=-\chi\frac{d}{dr}T_R^{4+\beta}, \tag{B8}$$

where

$$\chi=\frac{16\sigma}{3\overline{\kappa}(4+\beta)}$$

and $\overline{\kappa}=\kappa_0\rho^{1.3}$. Equations (B5) and (B8) can be combined and integrated. The result for cylindrical geometry is

$$\chi T_R^{4+\beta}=\frac{\epsilon(r_{Zob}^2-r^2)}{4}+\left(\frac{E_s}{2\pi L_Z\tau_{rs}}-\frac{\epsilon r_{Zob}^2}{2}\right)\left[\ln\left(\frac{r_{Zob}}{r}\right)\right]+\chi T_o^{4+\beta}, \tag{B9}$$

where T_o is the radiation temperature at the outer surface of the Z-pinch plasma. The result for spherical geometry is

$$\chi T_R^{4+\beta}=\frac{\epsilon(r_{Zob}^2-r^2)}{6}+\left(\frac{E_s}{4\pi\tau_{rs}}-\frac{\epsilon r_{Zob}^3}{3}\right)\left(\frac{1}{r}-\frac{1}{r_{Zob}}\right)+\chi T_o^{4+\beta}. \tag{B10}$$

APPENDIX C: SYMBOL DEFINITIONS

a	acceleration
a_2 and a_4	second- and fourth-order coefficients for mass/length of a Z pinch
α	axial convergence parameter ($\alpha=0$ for cylindrical pinches)
α_c and α_w	capsule and electrode wall albedos
A_Z	area of the Z pinch
A_n and B_n	Fourier coefficients to expand the mass/length of a Z pinch
β_s	average shock velocity over the average velocity of Z-pinch plasma
β	coefficient for power law fit to the opacity of gold
d_Z	thickness of the Z-pinch plasma at initial contact
ϵ	specific power within the Z-pinch plasma
E_A	energy available for heating after the collision
E_{cap}	the energy absorbed by the capsule
E_{int}	energy that goes into internal degrees of freedom
E_K	kinetic energy of Z-pinch plasma just before collision
E_{rad}	energy that is radiated from the dynamic hohlraum before capsule bang time
E_s	energy radiated from the outer surface of the Z-pinch plasma
E_w	radiation energy absorbed by the electrode wall
$E_Z(T)$ and $E_c(T)$	internal energy functions for Z-pinch plasma and the convertor
F_{op}	opacity multiplier
F_s	symmetry factor$=r_{Zib}/r_{cap}$
F_0	radiation source flux for view factor calculations without Rayleigh–Taylor
δF	radiation source flux for view factor calculations with Rayleigh–Taylor
δF_1	radiation source flux that produces 1% flux variation on the capsule
f_Z	fraction of the shock heating that goes into the Z-pinch plasma
γ	Gruneisen equation of state coefficient
$\Gamma(Z)$	thickness of the Z-pinch plasma with variations due to Rayleigh–Taylor
Γ_{min}	minimum thickness of the Z-pinch plasma
Γ_{Ross}	Rosseland mean of the Z-pinch plasma over thickness variations due to RT
I_p	peak drive current
κ	opacity
$\Lambda(Z)$	mass/length of a Z pinch
Λ_0	zeroth-order term in a Taylor expansion of the mass/length of a Z pinch
L_{hohl}	length of hohlraum for view factor radiation symmetry calculations
L_s	density scale length for RT growth rate
L_Z	the initial length of the Z pinch
λ	wavelength of the Rayleigh–Taylor instability
M_{cap}	initial capsule mass
$m_{cap}(r)$	unablated capsule mass as a function of radius as it implodes
M_c	mass of the convertor
M_Z	mass of the Z-pinch plasma
N_s	number of times a shock is driven through the convertor before capsule bang time
μ	shock convergence coefficient
P_{abl}	radiation induced ablation pressure
P_{ram}	ram pressure generated by ablated

	material interacting with the convertor
σ	Stefan–Boltzmann constant
r_{ab}	ablation stand off radius
r_{cap}	initial capsule radius
$r_c(t)$	capsule radius as a function of time
R_{ZH}	ratio of the spatial average of the radiation temperature in the Z-pinch plasma over T_{HP}
R_{hohl}	hohlraum radius for view factor radiation symmetry calculations
R_c	capsule radius for view factor radiation symmetry calculations
r_{Z0}	initial radius of the Z pinch
$r_{\mathrm{Z}}(t)$	radius of the Z pinch as a function of time
$r_{\mathrm{Zi}}(t)$ and $r_{\mathrm{Zo}}(t)$	radius of the inner/outer surface of the Z pinch as a function of time
r_{Zib} and r_{Zob}	inner/outer radius of Z-pinch plasma at capsule bang time
r_{co} and r_{ci}	initial outer/inner radius of the convertor
ρ_c	initial convertor mass density
$T_o(t)$	outer temperature of the Z-pinch plasma as a function of time
T_{ob}	outer temperature of the Z-pinch plasma at capsule bang time
t_p	time to pinch to the axis
t_r	rise time to peak current
τ_b	capsule bang time
τ_{cap}	capsule implosion time
τ_r	rise time to peak hohlraum temperature for annular convertors
τ_{rc}	effective radiation absorption time for the capsule
τ_{rw}	effective radiation absorption time for the electrode wall
τ_{rs}	effective radiation emission time for loss from the outer surface of the Z-pinch plasma
T_{HP}	peak hohlraum radiation temperature
$T_H(t)$	hohlraum radiation temperature as a function of time
$T_R(r)$	radiation temperature within the Z-pinch plasma
$v_s\overline{v_s}$	shock velocity and average shock velocity
v_{Zp} and $\overline{v}_{\mathrm{Zp}}$	Z-pinch velocity and average Z-pinch velocity
v_f	final capsule implosion velocity
V_{Z}	volume of the Z-pinch plasma

[1] R. B. Spielman, C. Deeney, and G. A. Chandler, Phys. Plasmas **5**, 2105 (1998).
[2] J. L. Porter, Bull. Am. Phys. Soc. **42**, 1948 (1998); R. J. Leeper *et al.*, Nucl. Fusion **39**, 1283 (1999).
[3] J. H. Hammer, M. Tabak, S. C. Wilks, J. D. Lindl, D. S. Bailey, P. W. Rambo, A. Toor, and G. B. Zimmerman, Phys. Plasmas **6**, 2129 (1999).
[4] J. H. Brownell and R. L. Bowers, Bull. Am. Phys. Soc. **40**, 1848 (1995).
[5] J. Lash, G. A. Chandler, G. Cooper, M. S. Derzon, M. R. Douglas, D. Hebron, R. J. Leeper, M. K. Matzen, T. A. Mehlhorn, T. J. Nash, R. E. Olson, C. L. Ruiz, T. W. L. Sanford, S. A. Slutz, D. L. Peterson, and R. E. Chrien, in *Proceedings of Intertial Fusion Science and Applications 99, Bordeaux, France, September 1999*, edited by C. Labaune, W. J. Hogan, and K. A. Tanaka (Elsevier, Paris, 2000), Vol. I, p. 583.
[6] J. H. Brownell, R. L. Bowers, K. D. Mclenithan, and D. L. Peterson, Phys. Plasmas **5**, 2071 (1998).
[7] I. V. Lisitsyn, S. Katsuki, and H. Akiyama, Phys. Plasmas **6**, 1389 (1999).
[8] J. Lindl, Phys. Plasmas **2**, 3933 (1995).
[9] G. B. Zimmerman and W. L. Kruer, Comments Plasma Phys. Control. Fusion **2**, 51 (1975).
[10] Y. B. Zel'dovich and Y. P. Raizer, *Physics of Shock Waves and High-Temperature Hydrodynamic Phenomenon* (Academic, New York, 1966), p. 52.
[11] G. B. Whitham, *Linear and Nonlinear Waves* (Wiley, New York, 1974), p. 198.
[12] K. S. Holian, ''T-1 Handbook of Material Properties Data Bases,'' Los Alamos National Laboratory, LA-10160-MS UC-34 November 1984.
[13] M. P. Desjarlais and B. M. Marder, Phys. Plasmas **6**, 2057 (1999).
[14] R. J. Leeper, R. E. Alberts, J. R. Asay *et al.*, *17th IAEA Fusion Energy Conference, Yokohama, Japan, October, 1998* [Nucl. Fusion **39**, 1283 (1999)].
[15] C. Deeney, M. R. Douglas, R. B. Spielman, T. J. Nash, D. L. Peterson, P. L'Eplattenier, G. A. Chandler, J. F. Seaman, and K. W. Struve, Phys. Rev. Lett. **81**, 4883 (1998).
[16] T. J. Nash, M. S. Derzon, R. J. Leeper, D. Jobe, M. J. Hurst, J. Seamen, and J. S. McGurn, Rev. Sci. Instrum. **70**, 464 (1999).
[17] R. E. Peterkin, Jr., M. H. Frese, and C. R. Sovinec, J. Comput. Phys. **140**, 148 (1998).